NANOIMPRINT LITHOGRAPHY FOR FUNCTIONAL POLYMER PATTERNING

A Dissertation

by

DEHU CUI

Submitted to the Office of Graduate Studies of
Texas A&M University
in partial fulfillment of the requirements for the degree of

DOCTOR OF PHILOSOPHY

December 2011

Major Subject: Electrical Engineering

NANOIMPRINT LITHOGRAPHY FOR FUNCTIONAL POLYMER PATTERNING

A Dissertation

by

DEHU CUI

Submitted to the Office of Graduate Studies of
Texas A&M University
in partial fulfillment of the requirements for the degree of

DOCTOR OF PHILOSOPHY

Approved by:

Chair of Committee,	Xing Cheng
Committee Members,	Jim Ji
	Hung-Jue Sue
	Jun Zou
Head of Department,	Costas N. Georghiades

December 2011

Major Subject: Electrical Engineering

ABSTRACT

Nanoimprint Lithography for Functional Polymer Patterning.

(December 2011)

Dehu Cui, B.S., Southwest Jiaotong University;

M.S., Pennsylvania State University

Chair of Advisory Committee: Dr. Xing Cheng

Organic semiconductors have generated huge interested in recent years for low-cost and flexible electronics. Current and future device applications for semiconducting polymers include light-emitting diodes, thin-film transistors, photovoltaic cells, photodetectors, lasers, and memories. The performance of conjugated polymer devices depends on two major factors: the chain conformation in polymer film and the device architecture. Highly ordered chain structure usually leads to much improved performance by enhancing interchain interaction to facilitate carrier transport.

The goal of this research is to improve the performance of organic devices with the nanoimprint lithography. The work begins with the controlling of polymer chain orientation in patterned nanostructures through nanoimprint mold design and process parameter manipulation, and studying the effect of chain ordering on material properties. Then, step-and-repeat thermal nanoimprint technique for large-scale continuous manufacturing of conjugated polymer nanostructures is developed. After that, Systematic investigation of polymer chain configuration by Raman spectroscopy is

carried out to understand how nanoimprint process parameters, such as mold pattern size, temperature, and polymer molecular weight, affects polymer chain configuration. The results indicate that chain orientation in nanoimprinted polymer micro- and nanostructures is highly related to the nanoimprint temperature and the dimensions of the mold structures.

The ability to create nanoscale polymer micro- and nanostructures and manipulate their internal chain conformation establishes an original experimental platform that enables studying the properties of functional polymers at the micro- and nanoscale and understanding their fundamental structure-property relationships. In addition to the impact on basic research, the techniques developed in this work are important in applied research and development. Large-area conjugated polymer micro- and nanostructures can be easily fabricated by thermal step-and-repeat nanoimprint for organic flat-panel displays, organic circuits and organic solar panels. The ability to manipulate chain orientation through nanoimprint presents a new route to fine-tune the electrical and photophysical properties of conjugated polymers, which can lead to improved performance for all organic electronics. The techniques developed here also allow for easy incorporation of other micro- and nanoscale soft functional polymers in miniaturized devices and systems for new applications in electronics, photonics, sensors and bioengineering.

To My Parents, Brother and Sister

This dissertation is lovingly dedicated to my parents, brother and sister, for their support, sacrifice and love throughout my life.

ACKNOWLEDGEMENTS

I would like to express my deep respect and gratefulness to my Ph.D. supervisor, Dr. Xing Cheng. Throughout my doctoral studies, he provided encouragement, sound advice, enthusiastic support, and lots of good ideas. I owe him lots of gratitude for making my research life enjoyable and rewarding. I also want to thank my committee members, Dr. Cote, Dr. Zou, Dr. Sue, Dr. Chang and Dr. Ji, for their guidance and support throughout the course of the research.

I wish to express my warm and sincere gratitude to all my lab buddies in Dr. Cheng's group, Hyunsoo, Huifeng and Taohua, for their friendship and help. They made the lab a convivial place to work.

Lastly, and most importantly, I wish to thank my family for their sacrifice, devotion, encouragement and providing a loving environment for me. They are always the source of courage and inspiration.

TABLE OF CONTENTS

Page

Page

LIST OF FIGURES

Page

Page

Page

Page

CHAPTER I

INTRODUCTION AND PRINCIPLES OF NANOIMPRINT LITHOGRAPHY

In recent years, the requirement for continuous device miniaturization in microelectronics has stimulated the development of new nanofabrication techniques [1]. Photolithography and electron beam lithography (EBL) have been the standard techniques for the microelectronic industry for years. At the same time, applications in electronics, optics and micro electromechanical systems also demand the ability to pattern the sub-100nm features and to form three-dimensional structures. Significant amounts of resources and research effort have been poured into the development of the next generation lithography systems. Among a number of novel lithography methods developed recently, nanoimprint lithography (NIL), initially invented and developed by the Chou group [2], has emerged as one of the most promising next generation lithographic techniques due to its high resolution, high-throughput, low cost, easy fabrication advantages.

Nanoimprint lithography (NIL) is a nonconventional lithographic technique. It relies on direct mechanical deformation of the resist material, and can overcome the resolution limitation imposed by the diffraction limits in both traditional and

---

This dissertation follows the style of *Advanced Materials*.

immersion photolithographic methods. NIL has stimulated great interest in both academic research and industrial development due to its high resolution, high throughput and low cost advantages [3].

1.1 Introduction

The features on the patterned mold can be replicated onto the resist materials via two different mechanisms, thermal nanoimprint and UV nanoimprint. The principle of thermal nanoimprinting can be simply defined as a mechanical forming technique that physically molds a deformable material into desired shape. Figure 1 illustrates the process procedures for thermal nanoimprint. In the thermal nanoimprint, a thin polymer film is spin-coated on the substrate. A pre-fabricated mold that contains nanoscale surface relief features is applied onto the film at controlled temperature and pressure, thereby creating a contrast in the polymeric material. A thin residual layer of polymeric material is often left underneath the mold protrusions. After cooling down, the template and the substrate are separated and the pattern is replicated on the substrate. For most applications, this residual layer needs to be removed by an anisotropic O_2 plasma-etching process to complete the pattern definition. There are varieties of materials ready for thermal nanoimprint, including functional materials, making thermal nanoimprint suitable for organic electronics and functional applications.

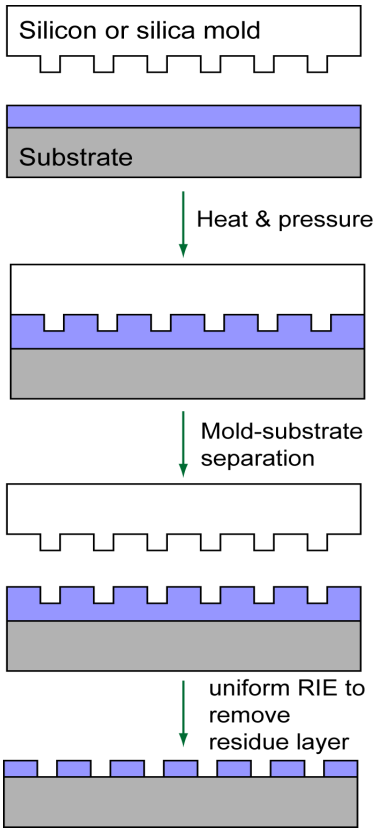

Figure 1. A schematic of thermal nanoimprint lithography.

Another method is ultraviolet nanoimprint (UV-NIL). This method forms the pattern by hardening liquid resist using UV radiation at low pressure. In UV-NIL, a transparent stamp with nano/micro-scale patterns is pressed on a thin resin layer or resin droplets and then UV light is exposed from above the stamp to cure the resin. After tens of seconds, in general, the stamp is separated from the patterned layer on the substrate; finally, anisotropic etching is used to transfer the patterns onto the substrate [4]. Figure 2 illustrates the process procedures for UV nanoimprint.

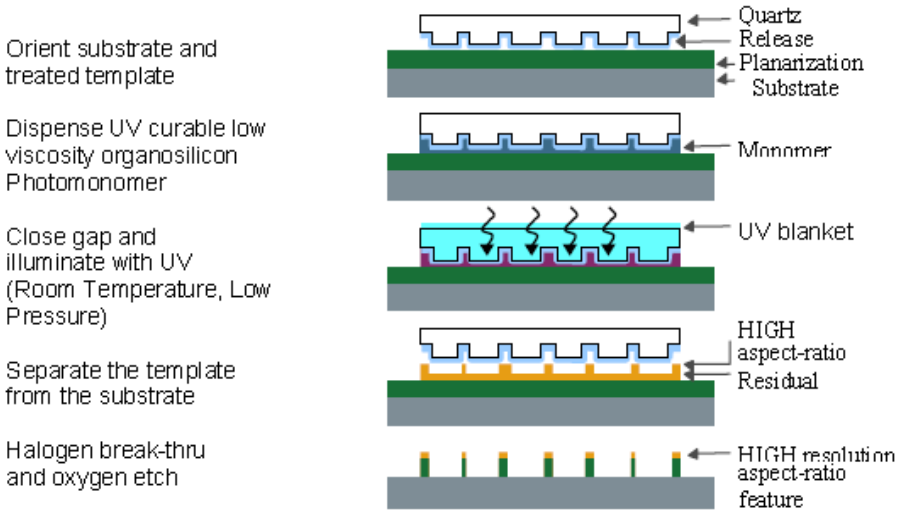

Figure 2. A schematic of UV nanoimprint [5].

Step-and-flash imprint lithography (S-FIL), which was developed by Willson's group, pattern replication is done in a step-and-repeat fashion. The schematic of the S-FIL is shown in Figure 3. The template is lowered onto the substrate, and irradiation with UV light through the backside of the template cures the solution. The template is then separated from the substrate leaving an organic-silicon relief image on the surface of the coated substrate that is a replica of the template pattern. The wafer is then stepped and the process is repeated on the next field. UV NIL eliminates the resolution limiting factors such as light diffraction and beam scattering that are often inherent with the more traditional lithographic approaches [5].

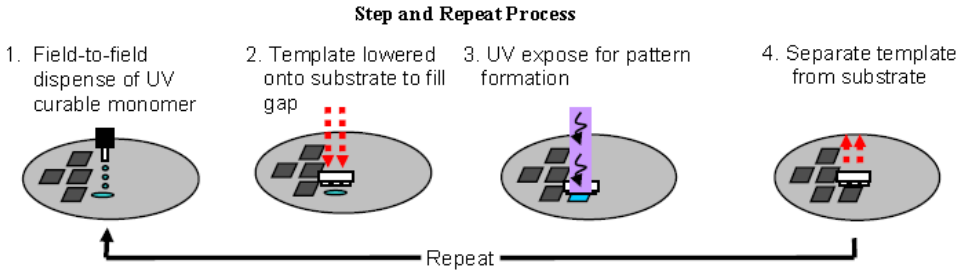

Figure 3. Step and repeat nanoimprint [6].

1.2 Nanoimprint template

The ability to fabricate micro to nanoscale nanoimprint template with high precision is of crucial importance to the development of the nanoimprint lithography. The semiconductor industry has been pushing high-precision nanoscale lithography to manufacture ever-smaller and higher-density features. The nanoscale structures are usually fabricated by, for example, high-resolution optical lithography and/or electron-beam lithography, followed by dry etching. Other patterning technologies such as interference lithography, tip-based direct writing, X-ray lithography and directed self-assembly process can also be utilized to prepare nanoimprint template.

Because nanoimprint temperature is usually over 100^{o}C, thermal mismatch between the mold and the substrate could result in pattern distortions and alignment errors. Thermal expansion coefficient, transparency, hardness, the compatibility with traditional microfabrication processing and the expansion coefficient are among the factors we need to think when choosing the material [6] for nanoimprint template. Hard nanoimprint mold have mostly been made of silicon (Si) or silicon dioxide (SiO_2) to

achieve high aspect ratio features, which has formidable resolution approaching 5 nm [7]. The advantage of Si or SiO_2 is due to its thermal expansion match with silicon substrates and its capability of being processed by a variety of dry etching process. Nickel is also a popular material for NIL due to its wide-spread usage in electroplating, but nickel mold and silicon substrate have thermal expansion mismatch issue [8]. Other materials for nanoimprint mold include diamond [9], silicon carbide [10]. Where the resolution and durability requirement is low, cross-linked polymer on silicon can also work as templates. Example materials include SU-8, Teflon and poly (dimethylsiloxane) (PDMS). The resolution achievable with PDMS has often been limited to >100 nm due to its relatively low compression modulus. Feng hua et al [11], showed that small diameter, single-walled carbon nanotubes can serve as templates for performing polymer imprint lithography with feature sizes as small as 2 nm - comparable to the size of a large molecule as shown in Figure 4. UV transparency is a must in UV nanoimprint, where quartz is a good choice. The quartz needs a releasing reagent on its surface because of the high adhesion with common photosensitive polymer.

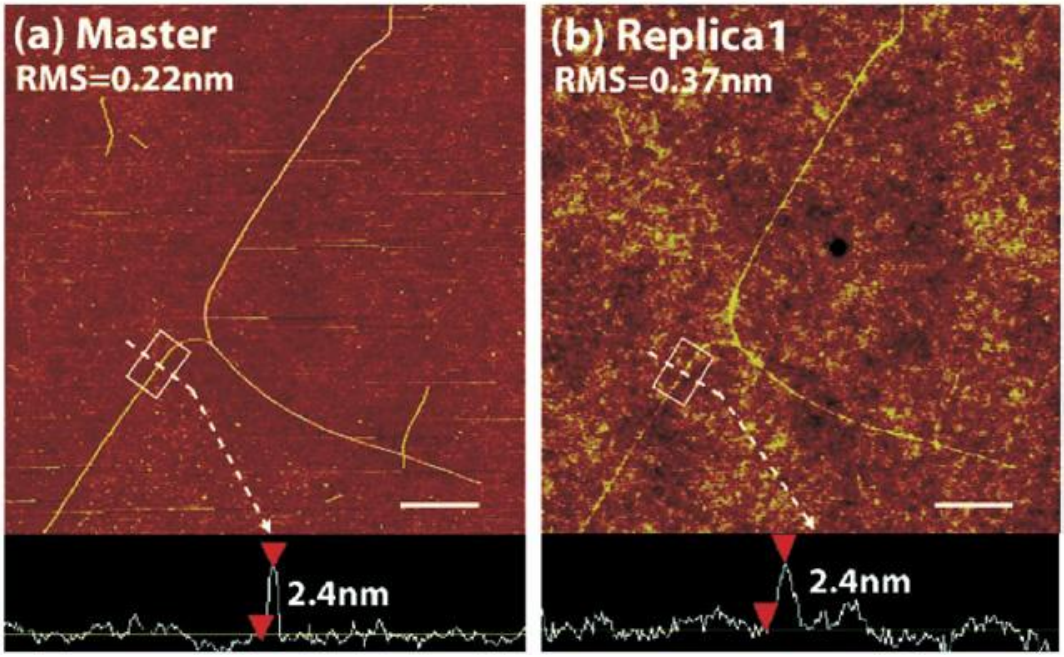

Figure 4. AFM images of a SWNT master and polymer nanostructures replicated by imprinting using the SWNT master [13].

1.3 Anti-adhesion coating for nanoimprint molds

A mold for imprint lithography typically has a high density of nanoscale protrusion features on its surface. This effectively increases the total surface area that contacts the imprinted polymer, leading to a strong adhesion of the imprinted polymer to the mold. One of the key issues of successful NIL technology is to avoid adhesion of the polymer to the stamp. Solutions to this problem are: [12]

(i) Incorporating an internal release agent into the resist,

(ii) Applying a low-surface energy coating to the mold;

(iii) Choosing a mold material with an intrinsically low surface energy.

The most widely adopted approach is to form a very good anti-adhesion property on either the stamp or the substrate. 1H,1H,2H,2H-perfluorodecyl-trichlorosilane (FDTS), which is well known as an anti-adhesion layer, can be coated on mold surface either by a solution-phase or a vapor-phase reaction. This approach can be readily applied to Si, or to oxide surfaces, to generate the required terminal hydroxyl groups. In vapor coating, after piranha cleaning and baking process, the mold is placed in a vacuum chamber. Surfactant are heated and evaporated to the mold surface. In solution phase coating, the surfactant is first mixed with a solvent such as heptanes. After that, the mold is immersed in the solution for about 10 minutes to form the surfactant coating. Compared to the flat substrates, the chosen deposition method is utterly important when working with nanometer-structured mold surfaces. Liquid phase deposition methods are disadvantageous due to insufficient wetting on the stamp material [8]. For nanostructures, surface tension and air pockets prevent solution from reaching the trench areas, which leaves the trench areas uncoated with surfactant. On the other hand, vapor coating method is easier to form surfactant coating regardless of the structure. Some researchers have claimed that vapor phase coating can provide better imprint results for nanoscale features [12]. The disadvantage of vapor coating is that this method requires vacuum system, which incurs higher cost compared to solvent coating method.

1.4 Resist materials in nanoimprint lithography

Nanoimprint is a mechanical deformation technique to replicate the mold structure onto a deformable material. There are a variety of materials suitable for nanoimprint lithography. For thermal nanoimprint, thermoplastic polymers are commonly used as nanoimprint resists. This choice can be explained by considering the typical deformation behavior of a thermoplastic polymer as a function of the temperature, as shown in Figure 5. The polymer exists in glassy state at low temperature. As temperature increases to the glass transition temperature, T_g, local motion of chain segments takes place and the modulus of the polymer drops by several orders of magnitude [13]. This is called the glass transition region. In this region, the polymer becomes soft and moldable. As temperature further increases, the polymer exhibits both rubbery and flow (viscoelastic) characteristics in the rubbery flow region. Finally, in the liquid flow region at even higher temperature, the polymer can flow like a liquid. Thermoset polymers can also be patterned by thermally curing the liquid precursor in-situ during nanoimprint.

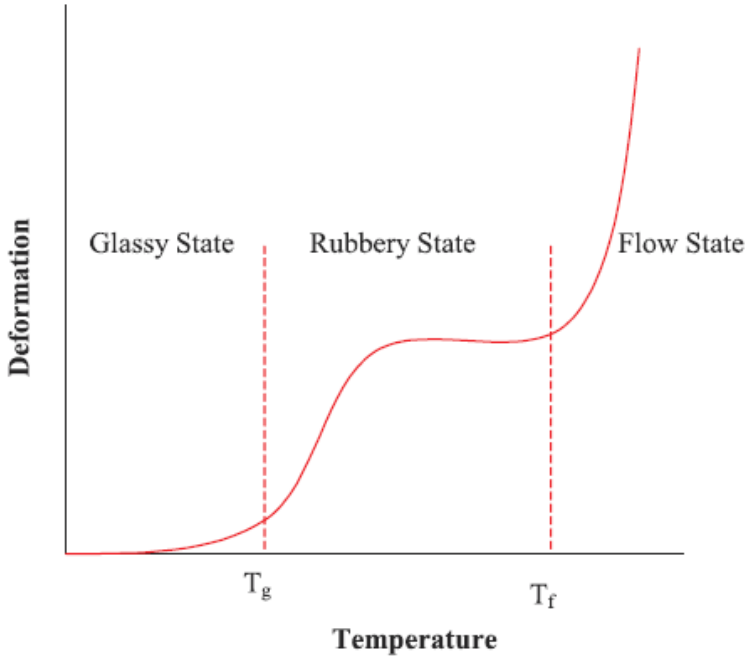

Figure 5. Typical deformation behavior of a thermoplastic polymer as a function of temperature.

In most cases, nanoimprint resist layer will be used as the mask layer further transfer the pattern into the substrate material and the resist layer will be removed after pattern transfer. However, in some applications, specialty polymers with unique properties can remain in the final device as active components after imprinting. Those polymers include functional polymers that combine multiple physical properties, such as mechanical, electrical, optical, acoustic, magnetic and chemical properties. In many MEMS applications, thermoset polymers also remain the final device and function as an indispensible component of the device.

The proper selection of a polymer is important to optimizing the NIL process and achieving stable and faithful pattern replication. For example, molar mass have a large effect on the physical, especially flow, properties of a polymer. Lower molar mass polymer having lower shear viscosity will tend to fill the mold more readily under given imprinting conditions [14]. On the other hand, a larger molar mass is important for fabricating stable ultra-small or high-aspect-ratio structures due to the better cohesive strength.

1.5 Nanoimprint Lithography Applications

As a generic lithography technique, NIL can be used for a lot of areas such as patterned tunable grating filter [15], bio chips[16], polymer waveguides[17], photonic crystals[18], micro-ring resonators[19], nanofluidic devices[20] and nanoelectronic devices[21]. For example, Figure 6 shows scanning electron microscopy (SEM) images of a mold with a pillar array (diameter 10 nm) and an imprinted 10 nm hole array in poly(methyl methacrylate) (PMMA) [22]. Figure 7 shows a uniaxial alignment of a liquid-crystalline conjugated polymer solar cell fabricated by nanoimprinting. The orientation of the conjugated backbones was parallel to the structures imprinted into the polymer film and parallel to the substrate, which lead to an increase in solar efficiency [23].

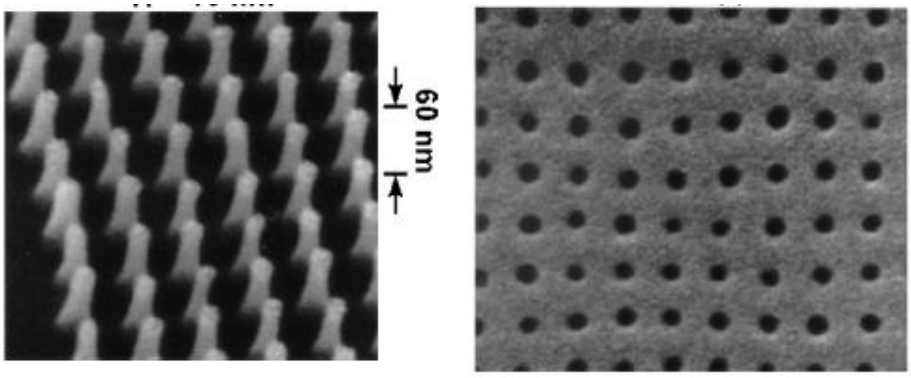

Figure 6. Scanning electron microscopy (SEM) image of a fabricated mold with a 10 nm diameter array in SiO_2 (left) and nanoimprinted 10 nm hole array in PMMA with the mold (right) [30].

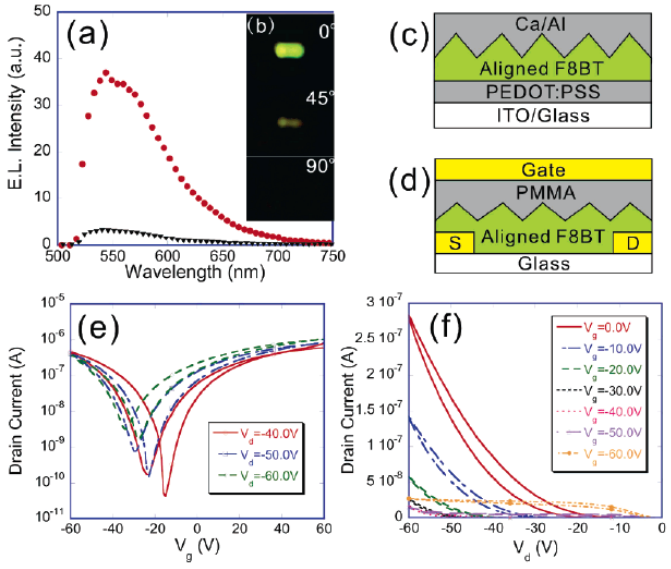

Figure 7. (a) Electroluminescent (EL) measurement of alignment polymer light-emitting diode (PLED). (b) Optical images of EL at different polarized angle of polarizer. (c) PLED device structure. (d) Polymer field-effect transistor (PFET) device structure using gold as electrodes. (e) Transfer characteristics of an aligned F8BT transistor. (f) Output characteristics of an aligned ambipolar F8BT transistor [31].

After a decade of intense research and development, NIL is already getting out of the laboratory and getting adopted by the industry. Molecular Imprints, Inc. (MII) has developed the ImprioTM 100 [5], which is the first commercial step-and-repeat imprint lithography system with field-to-field alignment. They pattered four fields at a time on a standard 6" mask wafer. Figure 8 shows a 200 mm wafer with well defined streets between the fields.

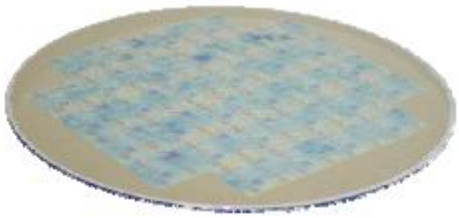

Figure 8. 200 mm wafer with well defined streets by MII [6].

NIL is cheaper and faster than other high-resolution lithography techniques such as e-beam lithography and AFM scratching in the fabrication of topographic patterns. In this study, we focus on thermal NIL with functional polymers. Compared with indirect patterning of a resist, where subsequent additive and subtractive processes are required, this direct patterning can minimize the required number of processing steps.

CHAPTER II

IMPROVING ORGANIC THIN-FILM TRANSISTOR PERFORMANCE BY NANOIMPRINT-INDUCED CHAIN ORDERING*

2.1 Introduction

Semiconducting polymers are conjugated polymers that have attracted enormous interest in research and development since their discovery [24]. Current and future device applications of semiconducting polymers include light-emitting diodes (OLED), thin-film transistors (OTFT), photovoltaic cells (OPV), chemical and biological sensors, photodetectors, lasers, and memory devices [25]. The versatility in tuning their electronic and optical properties by manipulating molecular structure through chemical synthesis has created a huge variety of conjugated polymers. This allows for intelligent material design to achieve best performance for specific applications. By combining attractive electronic and optical properties with common features of plastic materials such as flexibility, low cost, easy processing and mechanical robustness, conjugated polymers have the potential to enable novel large-area and flexible electric and optoelectronic systems, such as ultrathin and bendable emissive flat-panel displays, ubiquitous smart cards with integrated plastic circuits and flexible sensor arrays as artificial noses or skins for robotics.

---

* Part of this section is reprinted with permission from "Improving organic thin film transistor performance by nanoimprint-induced chain ordering" by Dehu Cui, Huifeng Li, Hyunsoo Park and Xing Cheng., 2008. *Journal of Vacuum Science & Technology B*, 26, 2404, Copyright 2008 by American Vacuum Society.

Although the potential of conjugated polymers are very promising, their widespread applications can be hindered by issues such as performance and reliability. Although OLEDs have shown good performance, the performance of OTFTs and OPVs are still considered low, which limit their commercial applications. The performance of conjugated polymer devices depends on two major factors: the chain conformation in polymer film and the device structure. Highly ordered chain structure usually leads to much improved performance by enhanced interchain interaction to facilitate carrier transport. On the other hand, scaling devices into nanometer scale can improve their performance, which is the basis for vigorous device scaling down in silicon microelectronics [26]. The motivation of this work is to address these two major factors in polymer electronics with the recent breakthrough in PI's research in nanoimprint lithography. To fully capitalize on the benefits of nanoscale organic devices such as better performance and higher integration density, it is also indispensable to develop low-cost fabrication techniques that are capable of patterning micro- and nanostructures over large areas on both rigid and flexible substrates.

Particularly OTFTs based on polymer semiconductors have been extensively studied because they can be fabricated by high-throughput and low-cost solution processing for ubiquitous electronic circuits. However, polymer OTFTs suffer low performance due to low carrier mobility [27]. Since the electronic and photophysical properties of polymer semiconductors are highly dependent on film morphology and polymer chain configuration [28], many techniques have been developed to enhance the carrier mobility by introducing ordered packing of polymer chains, such as

synthesizing regioregular polythiophenes [29] enhancing crystallization by liquid crystals [30], chain orientation by nanocomfinement [23], self-assembly [31], substrate texturing [32] and surface chemical treatment.

Recently, we observed ubiquitous polymer chain ordering in polymer micro- and nanostructures patterned by thermal nanoimprint. In thermal nanoimprint, the polymer film is heated to above its glass transition temperature [33] The applied pressure forces the polymer melt to flow and conform to the mold structure. Polymer materials exhibit chain ordering during melt processing [34] as illustrated in Figure 9(a). Anisotropy of material properties, such as refractive index, optical absorption and electronic transport, ensues after cooling, which locks the chain orientation in polymers. The formation of highly ordered chain packing in polymer materials is highly desired because the physical properties (e.g. mechanical strength and electrical conductivity) of oriented polymers are orders of magnitude higher than those of amorphous materials. [35] In thermal nanoimprint, polymer chain ordering originates from the polymer melt flow during pattern formation. Because the polymer flow field distribution in thermal nanoimprint depends on many nanoimprint parameters, such as the size, shape and depth of the mold structures, the polymer film thickness and the nanoimprint temperature, the actual chain orientation in polymer micro- and nanostructures can be complicated.

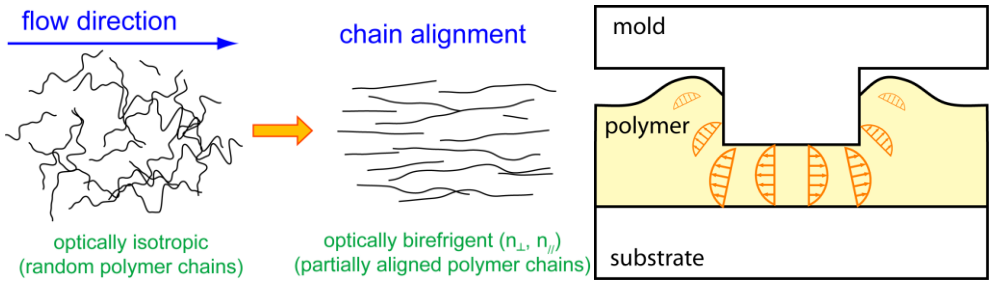

(a) (b)

Figure 9. Schematics of the origin of the chain orientation in polymer microstructures patterned by nanoimprint: (a) flow-induced chain orientation; (b) polymer melt-flow in nanoimprint.

Differences in deformation mode and replication fidelity have been attributed to a variety of factors, notably shear and extensional stretching, viscous flow and localized stress, residual stress release, shear-thinning and buckling, and surface tension. For a simple grating structure, the grating size is below micrometer, the polymer flow field can be represented by the simple schematic shown in Figure 9(b). The majority of chain orientation occurs under the mold protrusion area due to the extensional flow of the polymer melt in this region. In this work, we demonstrate the ability to achieve chain orientation in regioregular poly(3-hexylthiophene) (P3HT) gratings by thermal nanoimprint. Enhanced device performance is also achieved in OTFTs that are based on the nanoimprinted P3HT gratings.

2.2 Experimental details

The nanoimprint mold used in this work is 700-nm period grating with 50% duty cycle. The grating is replicated in a thermally grown oxide layer on a silicon substrate from a commercial holographic grating (Ibsen Photonics) by nanoimprint lithography and reactive-ion etching. The mold depth is 350 nm. The mold surface was coated with 1H,1H,2H,2H-perfluorodecyltrichlorosilane (FDTS) for anti-sticking and easy mold releasing.[36] For nanoimprint, regioregular P3HT films of around 260nm thick were prepared by spin-coating from dicholorobenzene solutions (20 mg/ml). The P3HT thickness after different spin coating speed was shown in Figure 10. All nanoimprints were done at 5×10^6 Pa for 5 minutes. The nanoimprint temperatures were varied from 100°C to 180°C.

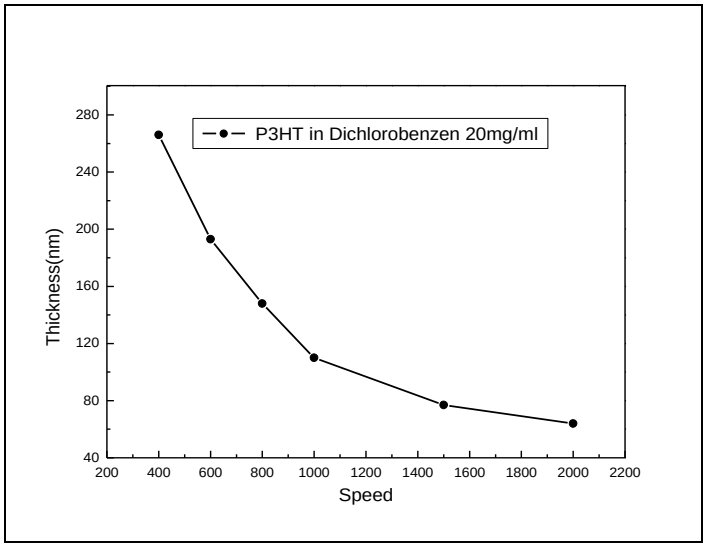

Figure 10. P3HT thickness as a function of spin coating speed.

The structural information of the P3HT gratings patterned by nanoimprint was investigated. Optical birefringence in P3HT grating was directly visualized in polarizing microscope with crossed-polarizers (Nikon Eclipse LV100POL). The crystalline phase inside the P3HT grating was probed by X-ray diffractometer (Bruker D8 Discover). Polarized absorption was measured with a spectrometer (Ocean Optics USB2000).

To evaluate the carrier transport in P3HT gratings, bottom-gate and bottom-contract OTFTs were fabricated with commonly used approaches. OFETs were fabricated on a heavily doped P-type Si wafer with a 100 nm thick thermally grown silicon oxide layer. The doped p-type Si functions as a gate electrode and the oxide layer as the gate dielectric. After standard photolithography to define the source and drain contacts, 5 nm titanium and 90 nm of gold were evaporated in sequence on the silicon oxide and lift off in a developer solution. P3HT film was then spin-coated on metal contacts and annealed at 140^{o}c for 5 minutes. The P3HT film was nanoimprinted with a grating mold at 150^{o}C and 5×10^{6} Pa. The current-voltage characteristics were measured by a semiconductor analyzer (HP 4155B). A P3HT OTFT nanoimprinted with a flat mold (no chain orientation) was used as a control device to ascertain the effect of chain orientation on device performance.

2.3 Results and discussion

P3HT is a semicrystalline polymer with a melting point around 240^{o}C [29]. This polymer represents an important class of conducting polymers due to its solubility,

processability, and environmental stability; it also possesses excellent electrical conductivity, electroluminescent properties. The unique processing characteristics and demonstrated performance of OTFTs suggest that they can be competitive candidates for existing or novel thin film transistor applications requiring large area coverage, structural flexibility, low temperature processing, and especially low cost [37]. As we known, varying the processing by allowing more time for crystallization or by changing the surface treatment causes the crystals to preferentially orient with their insulating side chains normal to the substrate and thus reduces the number of in-plane insulating grain boundaries and increases the charge carrier mobility [38].

In this work, though nanoimprints were done at temperatures lower than the melting point, polymer chains in amorphous regions can still flow under the heat and pressure. This process temperature have annealing effect on the polymer performance, it can increase the number of crystals with their side-chains oriented normal to the substrate. The annealed film also has an increased concentration of highly oriented crystals compared to the as-spun film. Furthermore, the stretching of the polymer chains in the nanoimprint will facilitate the interchain interactions. Ground and excited state interchain species, such as excimers and aggregates, may increase in the polymer film as a consequence of more ordered chain packing. It is also envisioned that the microcrystalline domains, which remain in crystalline phase at the nanoimprint temperatures, will reorient when the amorphous regions flow upon nanoimprint. All these factors will affect the chain configuration in polymer thin films and consequently their material properties.

2.3.1 Chain alignment in P3HT gratings patterned by nanoimprint

In P3HT gratings patterned by nanoimprint, the polymer chains will be stretched and aligned in the direction perpendicular to the grating ridges and trenches, which leads to optical birefringence in the directions perpendicular and parallel to the grating lines. The optical birefringence can be directly observed in polarizing microscope with crossed-polarizers. If the incident light is polarized parallel or perpendicular to the chain stretching direction, the polarization state of the incident light will be unaffected. After exiting the P3HT film, the polarized light will be completely blocked by the top polarizer, leading to a dark image of the sample. When the P3HT grating is rotated by an angle, the incident polarized light will see the optical birefringence in the film. The birefringence will rotate the polarization direction of the incident light. After propagating inside the film, the incident light will develop a net component along the polarization direction of the top polarizer, leading to a bright image of the sample.

The polarizing microscope images of P3HT gratings patterned by nanoimprint at 100^{o}C, 150^{o}C and 180^{o}C are shown in Figure 11(a), (b) and (c) respectively. In all P3HT gratings, dark images are observed when the grating lines are either parallel (0^{o}) or perpendicular (90^{o}) to the polarization direction of the incident light. As the gratings are rotated away from the polarization direction of the incident light, images emerge gradually brighter. Maximum brightness is observed at 45^{o}. Those observations clearly demonstrate the optical axes of the birefringence in P3HT gratings are parallel and perpendicular to the grating lines. This is consistent with the

chain stretching direction in thermal nanoimprint and indicates that the polymer melt flow is the cause of the observed birefringence.

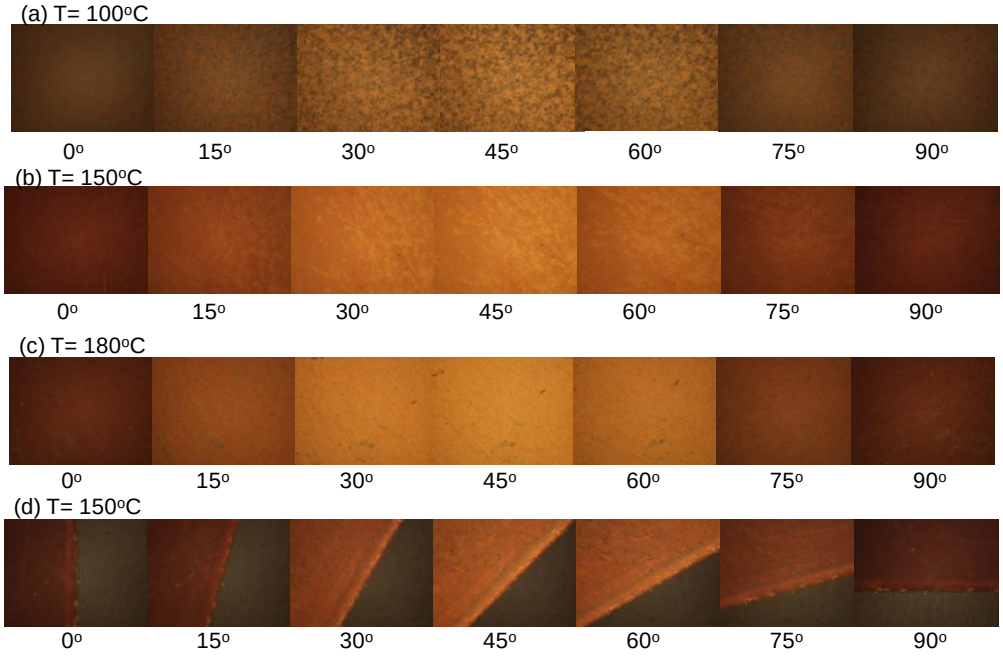

Figure 11. Polarizing microscope images of P3HT gratings patterned by nanoimprint at 100°C (a), 150°C (b) and 180°C (c). Part (d) shows the edge area of the P3HT grating patterned at 150°C.

In Figure 11, it is also observed that better chain orientation is achieved at higher nanoimprint temperature. The P3HT grating nanoimprinted at 100°C shows dark spots (amorphous regions) when the sample is rotated by 45°. At 150°C, the dark spots disappear but inhomogeneity exists in the P3HT gratings. At 180°C, a more uniform chain orientation is observed. Polymer chains are more flexible at higher temperature, thus nanoimprint at higher temperature can result in better chain

orientation. The conclusion that chain orientation originates from melt flow can be corroborated by the observation in Figure 2(d), which shows the edge of the grating area after nanoimprint at 150^{o}C. The area without grating structures, which underwent the same thermal history as the grating area, does not exhibit birefringence. The amorphous regions and the randomly oriented microcrystallines make the P3HT film be optically isotropic, which appear as the dark area in Figure 11(d). Nanoimprint induces optical birefringence in grating (bright) area by stretching the polymer chains in amorphous region and by reorienting the microcrystalline domains.

2.3.2 X-ray diffraction spectra of patterned films

Dyreklev et al reported that in an OTFT having an aligned poly(3-octylthiophene) film as the active layer, there is a correlation between the polymer stretching ratios and the mobility. Highly aligned polymers are interesting for the preparation of both organic LEDs and TFTs with enhanced properties [39]. X-ray diffraction (XRD) is a powerful tool to provide information on the spacing and orientations of crystal planes; it can be used to measure the crystal planes with lattice vectors normal to the surface and samples the entire thickness of the film.

The internal chain packing in the P3HT gratings can be probed by the XRD technique. Figure 12 shows the XRD spectra of the as-deposited P3HT film (Figure 3(a)) and the P3HT gratings processed at 100^{o}C (Figure 12(b)), 150^{o}C (Figure 12(c)) and 180^{o}C (Figure 12(d)). The P3HT (100) peaks have higher intensity in gratings than that in the as-deposited film. Progressive increasing of the (100) peak intensity is

also observed as nanoimprint temperature increases. The increased peak intensity may come from the reorientation of the microcrystalline domains or the annealing effect during nanoimprint.

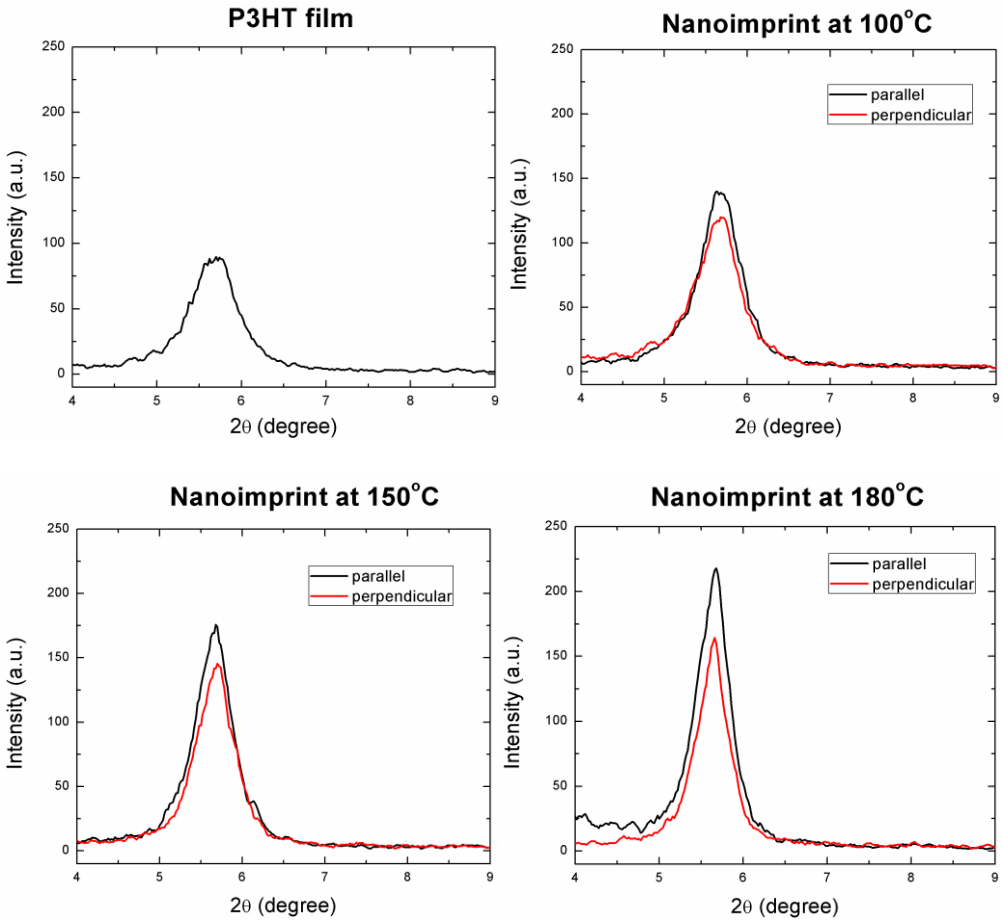

Figure 12. XRD spectra of the as-deposited P3HT film (a) and the P3HT gratings patterned by nanoimprint at 100°C (b), 150°C (c) and 180°C (d).

In the nanoimprint process, as the mold is pushed into the polymer film, the polymer flows along the mold surface. The polymer film under the mold is heavily

compressed and most of them are extruded from the original positions in the horizontal direction. This process is like as the stretching process. A stress field applied to this polymer would cause the crystallites to orient by rotations and the amorphous phase to orient as an amorphous polymer with the restriction that many of the amorphous chains are physically cross linked by the crystallites [40]. Shear deformations are most happened near the stamp surface and corner, the polymer is extending along the mold side due to the friction force, which flow upwardly and fill the cavity of the mold. The polymer is also extended in the upward direction. At the end of the imprint process, Due to the compression of polymer film, high density areas are concentrated under the stamp pattern and, as a result, a large stress is generated at the polymer surface and manifestly birefringence effect also arise in this region.

We found that as the temperature increases, the peak of the patterned P3HT peak become more intense and sharper. But in the vicinity of the melting point, the peaks begin to decrease in intensity, and once above the melting temperature, they decrease much more. The peak changes between low and high temperatures may be due to thermal expansion along the gratings. The integrated intensity increases gradually in the low temperature region and then decrease as temperature approaches the melting point. The slightly narrower peak in the P3HT grating patterned at 180^{o}C indicates that the reorientation of the microcrystalline domains is at least a partial factor that leads to the observed ordering in the P3HT gratings. A difference in the (100) peak intensities between two reference directions (parallel and perpendicular) is also observed in all P3HT gratings. This difference most likely stems from the

microcrystalline reorientation in P3HT films after nanoimprint. However, more detailed study is needed to rationalize the details of the XRD peak intensity change.

2.3.3 Polarized absorption spectra of patterned films

The chain morphology change in P3HT gratings has a direct impact on the photophysical properties of the conjugated polymer films. The polarized absorption spectra of the P3HT gratings nanoimprinted at 100, 150, and 180 ℃ are shown in Figs. 13(a)–13(c), respectively. Figure 13(d) illustrates the polarization directions of the incident light. In each grating, higher absorbance is observed when the incident light is polarized perpendicular to the grating lines. Since the chain stretching direction is also perpendicular to the grating lines, this indicates that higher absorption occurs when incident light polarization aligns with the chain orientation direction. More careful examination of the absorption spectra reveals a red-shift of the peak absorbance as nanoimprint temperature increases. The red-shift of the absorption spectrum indicates further delocalization of electrons due to the formation of aggregates in conjugated polymer film [28] . It can be explained as a result of chain stretching and orientation after nanoimprint because extended linear polymer chains allow better interaction among chains to form interchain species such as aggregates.

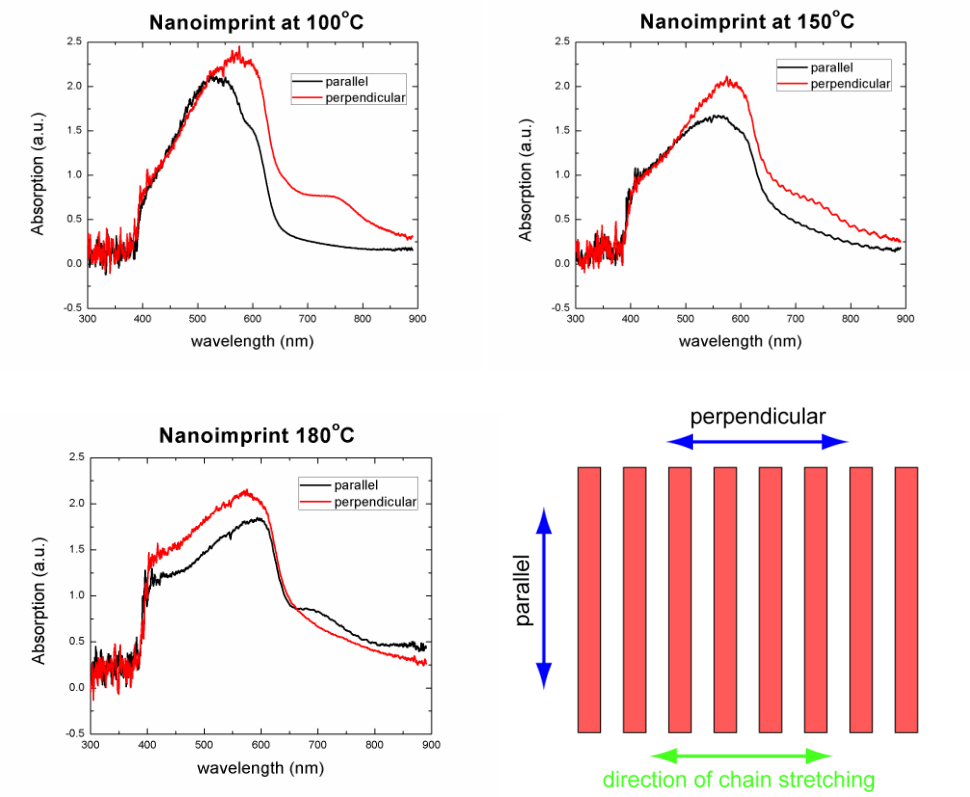

Figure 13. Polarized absorption spectra of the P3HT gratings patterned by nanoimprint at 100°C (a), 150°C (b) and 180°C (c). Part (d) illustrates the incident light polarization directions.

2.3.4 OTFTs based on nanoimprinted P3HT gratings

The interchain species formed after nanoimprint also facilitate the carrier transport in conjugated polymer films, thus enhance the performance of OTFTs based on these chain-aligned P3HT gratings. The schematic of a bottom-gate and bottom-contact OTFT with P3HT grating is shown in Figure 14(a). The polarizing microscope image of the device in Figure 14(b) shows chain orientation in the nanoimprinted

P3HT grating. Based on the device structure in Figure 14(a), the carrier transport will occur in the residual layer at the bottom of the film. The chain-aligned bottom residual layer is about 85 nm thick.

After the nanoimprint, the anisotropic material is stretched in the perpendicular direction. The random- coil conformation of the polymer chains is distorted in the stretching process and the macromolecules become extended and aligned. Alignment of the polymer chain will give us an electronically anisotropic material since the dipole transitions are oriented along the main chain direction [41].

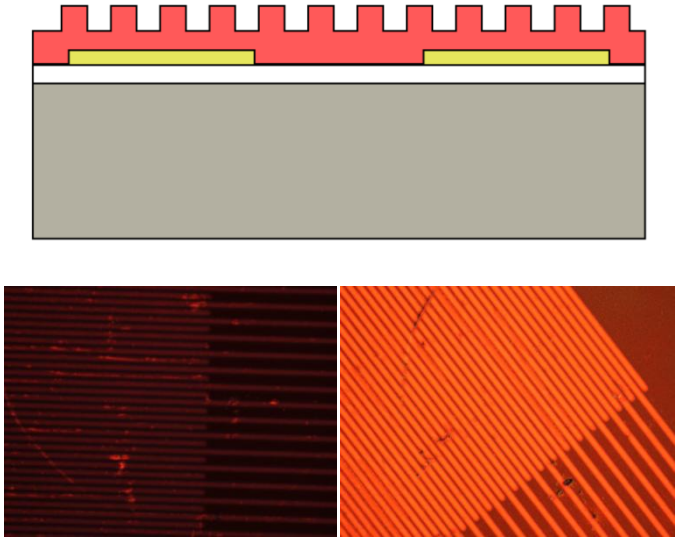

Figure 14. (a) A schematic of a bottom-gate and bottom-contact OTFT based on nanoimprinted P3HT gratings; (b) Polarizing optical microscope images of the fabricated devices. The angles between the grating lines and the incident light polarization direction are 0^{o} and 45^{o} in dark and bright images respectively.

Initial conjugated polymers were intractable due to the lack of side chains. The addition of side chains lowers the melting temperature and increases the solubility by separating the conjugated backbones and the reducing the rigidity of the backbone. The separation of the backbones by the side chains reduces the intermolecular overlap, and thus impedes hopping of charges between molecules. Since the chain length of polymer molecules is considerably less than the channel length of TFTs or the thickness of diodes, charges traveling through a film must hop between molecules to get from one electrode to the other. Hopping between molecules is related to the intermolecular overlap of neighboring molecules, which is clearly dependent on how molecules pack on each other. Additionally, conjugated molecules are typically longer than the persistence length, so a charge is not expected to be able to travel the full length of a molecule before having to hop to a neighbor. The persistence length in a solid state film is generally also related to the chain packing. Therefore the chain packing is critical to charge transport.

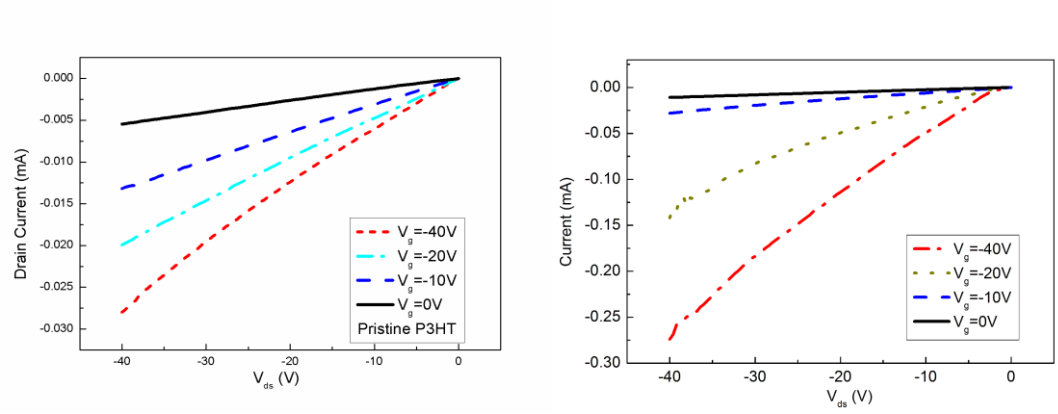

Figure 15. The output characteristics of the OTFTs based on the as-deposited P3HT (a) and the P3HT gratings patterned by nanoimprint at 150^{o}C (b).

Figure 15(a) and (b) respectively show the output characteristics of the control device (without chain orientation) and the OTFT with the P3HT grating patterned at 150^{o}C at different gate biasing level. The drain current is significantly enhanced for the nanoimprinted OTFT compared with the control device. The hole mobilities were extracted from the transconductance values in the linear region. Hole mobilities in the control device and the grating OTFT are 1.35×10^{-3} cm^2/Vs and 1.62×10^{-2} cm^2/Vs respectively. More measurements reveal that the carrier mobility in the direction perpendicular to chain stretching is about two times of that in parallel direction.

The structural and material property changes in P3HT gratings revealed by polarizing microscope, XRD, polarized absorption and thin-film transistors show nanoimprint can be a useful technique in tuning the properties of conjugated polymers by controlling the internal chain configurations. Systematic studies are needed to investigate the factors that affect the chain orientation in polymer microstructures in order to achieve maximum impact on device performance. For example, all nanoimprints in this work were done below the P3HT melting point. Further modification of chain configuration can be achieved by nanoimprint at temperatures higher than the P3HT melting point. In this situation, the microcrystalline phase will be destroyed and more uniform chain orientation can be achieved. In addition to achieve better chain orientation in polymer films, the stability of the chain orientation in polymer microstructures should also be evaluated because chain orientation in P3HT grating is thermodynamically meta-stable. Post-nanoimprint annealing may lead to the reorganization of the polymer chains. Although the relaxation of the chain

orientation presents problem to the structural stability of polymer nanostructures, annealing after chain stretching may lead to conjugated polymer films with higher crystallinity and better performances.

2.4 Summary

In summary, we have demonstrated that the polymer chain configuration in polymer films can be manipulated by thermal nanoimprint. Polarizing microscope images show strong optical birefringence in P3HT gratings patterned by thermal nanoimprint. The optical axes of the birefringence are parallel and perpendicular to the grating lines, which is consistent with the chain stretching direction in these gratings. The origin of the optical birefringence comes from the stretching of polymer chains when polymer flows during pattern formation in nanoimprint, as demonstrated by the fact that only patterned area has optical birefringence. XRD spectra of the P3HT gratings reveal better orientation of the microcrystalline phase at higher nanoimprint temperatures. Polarized absorption spectra show higher absorption along the chain stretching direction. The observed anisotropy in thin film properties can be explained as a consequence of both chain orientation in amorphous region and the reorientation of the microcrystalline domains. OTFTs based on P3HT gratings have nearly twelve times higher mobility compared to the control device without chain alignment. This result indicates nanoimprint can be a powerful yet simple tool to improve the performance of organic electronics. Further optimization of nanoimprint processing parameters will be developed in future to provide a better understanding of the

nanoimprint-induced chain ordering phenomenon. It is noteworthy to point out that the approach developed in this work can be broadly extended to many other functional polymers to improve their performance, which opens up new horizons for nanoimprint applications.

CHAPTER III

STEP-AND-REPEAT SOLID-PHASE NANOIMPRINT FOR HIGH-THROUGHPUT FUNCTIONAL POLYMER PATTERNING

3.1 Introduction

In recently years, the need for low-cost and high-throughput nanopatterning has stimulated the fast development in nanoimprint lithography (NIL)[8, 33, 42, 43] One of the major research focuses in nanoimprint development is to improve process throughput for large-scale nanopatterning over large areas for commercial applications. Based on materials used and processing schemes, NIL can be classified into two types: thermal NIL [22, 44] and ultraviolet NIL (UV-NIL) [45]. UV-NIL has gained more attention, particularly for commercial nanofabrication in microelectronic industry, than thermal NIL because it can be implemented in a step-and-repeat fashion (e.g., Step-and-Flash Imprint Lithography [43, 46] for nanopatterning over a large substrate with low-cost and high-throughput. Such step-and-repeat mechanism cannot be implemented in thermal NIL because subsequent NIL requires heating to above the glass transition temperature (T_g) of the polymer resist, which will inevitably destroy the nanostructures formed in preceding nanoimprints. Since thermal NIL is gaining increasing attention in direct patterning of conjugated and piezoelectric polymers with the capability of manipulating nanoscale chain orientation and crystallization [47, 48], it is highly desirable to achieve the step-and-repeat capability in thermal NIL for large-area functional polymer patterning.

Although room temperature nanoimprint of thermoplastic polymers [49, 50-52, 53], which can be implemented in a step-and-repeat fashion,[50] has been performed based on the principles of free volume compression in amorphous polymers followed by stress-induced plastic yielding [52], it usually requires much greater pressure and pattern replication is often incomplete, particularly for larger dimensions. It is also expected the temperature stability of those amorphous polymer structures patterned under very high pressure at room temperature is poor due to free volume restoration and polymer chain recovery. Room-temperature nanoimprint and multi-step imprinting at the same location have been demonstrated using low-density polystyrene [53] or low molar-mass conjugated oligomers [51]. Room-temperature nanoimprint can also be done by lowering polymer modulus through solvent damping [54] or plasticizing [55]. However, such techniques are not convenient to perform, and they are not compatible with the step-and-repeat scheme because prolonged exposure to solvents or plasticizers can lead to pattern decay. The need for additives in polymers to achieve direct patterning below polymer T_g is not desirable, particularly for conjugated polymers such as poly(3-hexylthiophene-2,5-diyl) (P3HT) because external materials often interfere with their electrical properties. In this communication, we present solid-phase thermal NIL at elevated temperature for step-and-repeat patterning of thermoplastic functional polymers without the need for excessive imprint pressure.

3.2 Experiment

For solid-phase thermal nanoimprint, grating mold with 700 nm period, 50% duty cycle, and 350 nm depth were fabricated in thermally grown silicon oxide. The patterns were defined by electron-beam lithography. The grating structures were etched into the oxide layer by reactive-ion etching with CHF_3 gas with Cr as the hard mask in Oxford Plasmalab System 100. After piranha cleaning (sulfuric acid: 30% hydrogen peroxide = 3:1) for 30 minutes, the mold was coated with 1H,1H,2H,2H-perfluorodecyltrichlorosilane (FDTS, from Gelest Inc.) in a Petri dish that contains dilute solution of FDTS in heptane for mold releasing after nanoimprint. The mold was baked on hot plate at 110^{o}C for 10 minutes to further crosslink Si-O-Si bonds.

3.2.1 Nanoimprint mold fabrication

Figure 16 described the successive steps of repeating mold by nanoimprint lithography. In the first step, 180nm thickness Poly (methylmethacrylate) (PMMA, molecular weight 15k) was spin coated on the silicon oxide wafer, the nanoimprint were done at 5×10^{6} pa at the 175 ^{0}C for 5 minutes. The residue can be moved by oxygen reactive-ion etching (RIE). Second, a 50nm Cr was evaporated on the patterned PMMA surface, followed by a lift off process to remove the resist and leave the metal on the top. Then the patterns were transferred into silicon oxide by CHF3 RIE with the depth abound 350nm. After that, the Cr film will be removed. The mold surface was coated with 1H,1H,2H,2H-perfluorodecyltrichlorosilane by a solution-phase reaction for anti-sticking and easy mold releasing.

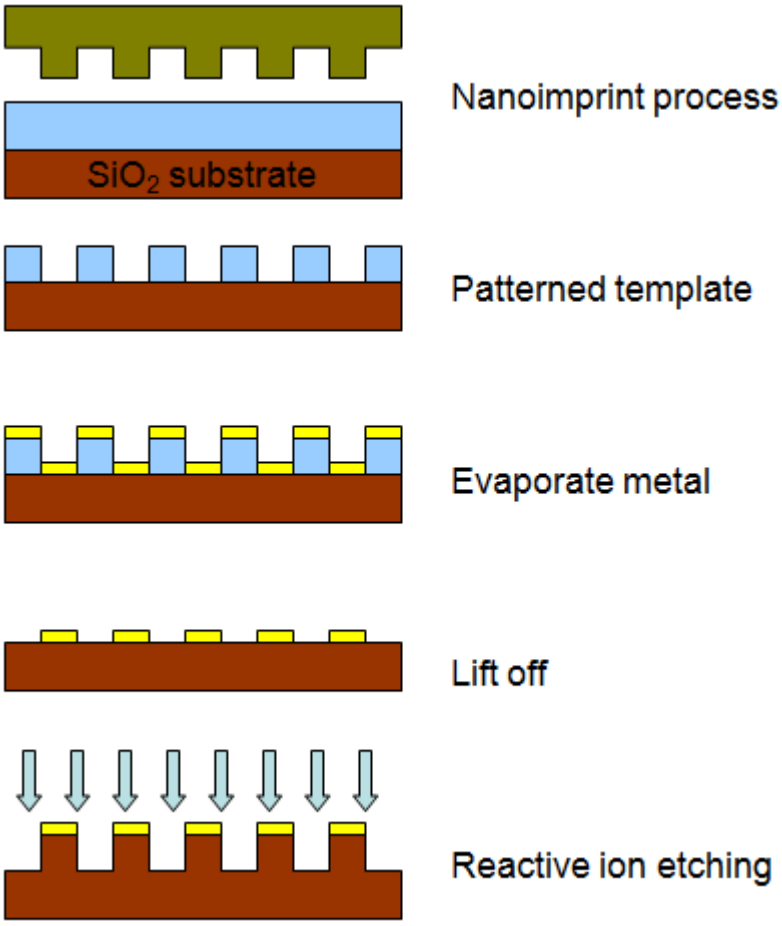

Figure 16. A schematic illustration of the SiO_2 mold fabrication process.

3.2.2 Step-and-repeat Nanoimprint

P3HT (Rieke Metals, P-200, average $M_w \approx 50$ kg mol^{-1}) solution in dichlorobenzene (20mg/ml) was first spin-coated on a Si wafer to achieve a film thickness of 200 nm. The nanoimprint process was carried out at 150^{o}C with a pressure of 5 MPa between two parallel platens. After separating the mold from the

substrate, the mold was moved to an adjacent area on the same substrate to perform the next nanoimprint.

By taking advantage of the yielding behavior of semicrystalline polymers, solid-phase NIL can be performed on a single substrate many times in a step-and-repeat fashion, as shown in Figure 17, without destroying the patterns formed in preceding nanoimprints. The first nanoimprint is performed using a mold on a much larger substrate at a temperature that is lower than the polymer T_g or melting temperature T_m (Figure 17(a)). Pattern formation is achieved through stress-induced polymer yielding. After the first nanoimprint, the mold is separated from the substrate and moved to a new location while the temperature is kept constant. The nanoimprint can be performed again by applying a pressure.(Figure 17(b)) Such scheme can be repeated many times to complete the patterning of the large substrate (Figure 17(c)). All nanoimprint processes, including demolding, can be performed at a constant temperature with the elimination of the heating and cooling cycles.

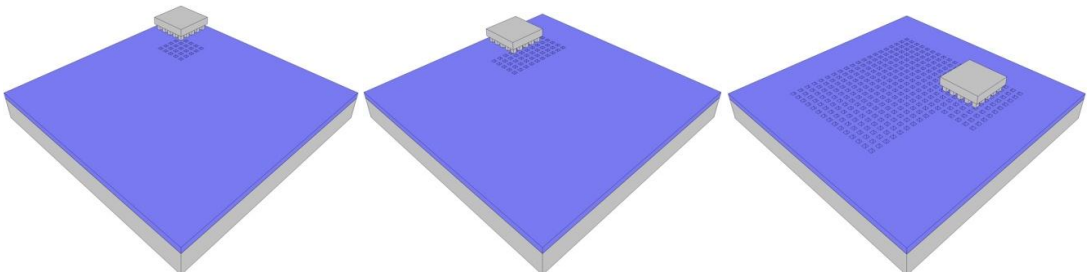

Figure 17. A schematic of the solid-phase step-and-repeat thermal nanoimprint.

Characterization of nanoimprinted functional polymer structures: The SEM images of the nanoimprinted P3HT patterns were obtained by JSM-7500F ultra high resolution field-emission SEM. Optical birefringence was observed in a Nikon polarizing microscope model POL 150. The polarized absorption spectra of the nanoimprinted P3HT patterns were recorded with Ocean Optics USB4000-UV-Vis spectrometer.

The 700 nm period grating mold with 350 nm depth and 10 μm period grating mold with 0.8 μm depth for nanoimprint was fabricated in 1.0 μm thick thermal oxide on silicon substrate. The patterns are defined by electron-beam lithography and photolithography for 700 nm and 10 μm period gratings respectively. The grating structure is etched into the thermal oxide layer by RIE with CHF_3 gas. The molds were coated with FDTS to render the mold surface hydrophobic for easy mold releasing. The low surface energy is also needed for the dewetting process to occur. The molds were cleaned by piranha solution (sulfuric acid: 30% hydrogen peroxide = 3:1) for 30 minutes before FDTS coating. The coating was done by soaking the molds in heptane with a few drops of FDTS for 10 minutes.

All polymer films (15k and 75k PMMA, MEH-PPV and P3HT) are prepared from spin-coating of polymer solutions. To reduce polymer-substrate adhesion for easy transfer of polymer film onto mold surface after nanoimprint, the silicon substrates were first coated with OTS. The OTS coating procedure is the same as that of FDTS. Soft bake was done at 95 ℃ for 2 minutes on hotplate to remove solvent in films after spin-coating. For the layer-transfer, the polymer film on the substrate was

imprinted at 175 ℃ for 5 minutes with 5×10^6 Pa and then this pressure was maintained until the temperature falls to room temperature. After releasing pressure, polymer layer was transferred to the mold by slight twisting of mold against substrate. Unlike conventional vertical separation of the mold and substrate assembly, the polymer film was detached from substrate and attached on mold surface.

3.3 Result and discussion

A schematic of the stress-strain curve for a semicrystalline polymer is shown in Figure 18. The linear line from point A to point B is the elastic response of the polymer. When the applied stress reaches the yield stress of the polymer at point B, the semicrystalline polymer begins to deform through internal chain reconfiguration. The deformation continues while the stress remains relatively constant until strain-induced hardening sets in, and stress starts to gradually increase to reach point C. At point C, the external stress is removed and a small elastic recovery of the stretched polymer occurs, as indicated by the line from point C to point D. Point D represents the final irrecoverable strain of the polymer, and the distance between point D and the origin (point A) represents the permanent deformation of the polymer. The solid-phase NIL achieves pattern formation in semicrystalline polymers through yield-induced deformation, which is fundamentally different from traditional thermal nanoimprint where viscoelastic polymer melt flow contributes to pattern formation [33]. Solid-phase NIL is analogous to cold forming techniques [56] such as cold forging, cold drawing [57],

and cold extrusion [58], used in polymer industry to process polymers that are difficult for melt processing due to high molecular weights.

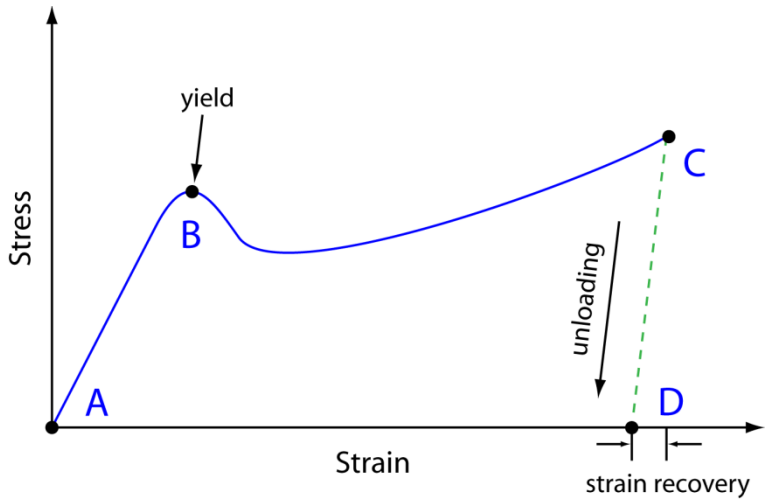

Figure 18. A schematic of the stress-strain curve for a semicrystalline polymer.

3.3.1 SEM images of the P3HT

Regioregular P3HT, widely used for polymer thin-film transistors and solar cells, is a semicrystalline conjugated polymer that has the mechanical property suitable for solid-phase thermal NIL. Figure 19 shows the P3HT gratings with 700 nm period and 50% duty cycle patterned by four consecutive nanoimprints on the same substrate in a step-and-repeat fashion. The mold and the substrate were placed between two heated parallel platens in ambient environment. All nanoimprint were done at 120^{o}C with a pressure of 5 MPa. The nanoimprint temperature is below the melting temperature of P3HT, which is ~ 225^{o}C. [59] The scanning electron microscope

(SEM) images for the four nanoimprints are shown in Figure 19. 4 (a), (b), (c) and (d), respectively. It is clearly seen that grating patterns are well formed in all nanoimprints. The grating formed in the first nanoimprint (Figure 19(a)), which was subjected to heating during following nanoimprints, is almost the same as the fourth nanoimprint (Figure 19(d)). The well-formed P3HT gratings and the preservation of the line-edge roughness, which comes from the lift-off process during mold fabrication, indicate no pattern reflow or decay occurred during subsequent heating. A photograph of the substrate with four nanoimprinted pads is shown in Figure 19(e). The four colored regions are the P3HT gratings and the dark areas correspond to P3HT film with no grating pattern. Defect regions are also seen on the substrate, which originate from non-conformal contact between the mold and the substrate because all nanoimprints were performed between parallel platens in ambient environment.

The yielding of semicrystalline polymers is concomitant with polymer chain stretching and alignment. Chain stretching not only contributes to the deformation of the polymer materials, but also enhances mechanical properties due to improved interchain interactions for polymers with rigid backbones. Such feature grants structural stability of the nanoimprinted patterns and ensures that no pattern relaxation will occur even when the patterns are kept at the nanoimprint temperature. Strong optical birefringence was observed in all P3HT gratings patterned by the solid-phase nanoimprint with a polarizing microscope. This is similar to the case in which P3HT was nanoimprinted at higher temperature [47].

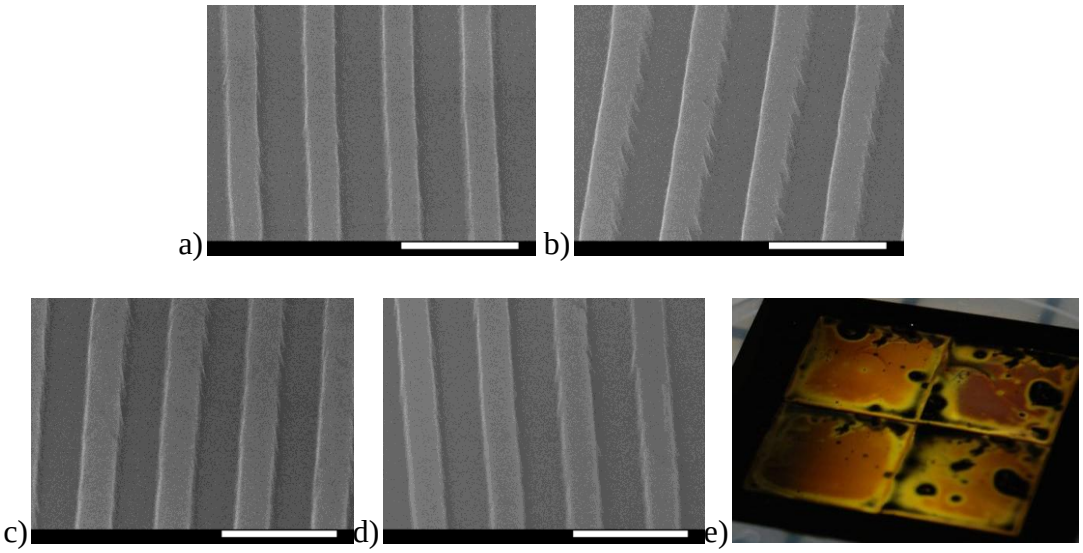

Figure 19. SEM pictures of the P3HT gratings of 700 nm period and 50% duty cycle from (a) the first nanoimprint, (b) the second nanoimprint, (c) the third nanoimprint and (d) the fourth nanoimprint. No pattern degradation is observed in P3HT grating after multiple nanoimprints on the same substrate. Scale bar: 1 μm. (e) Photography of a substrate with four nanoimprint pads.

3.3.2 Absorption spectra of P3HT patterned by step-and-repeat thermal nanoimprint

Chain stretching also yields anisotropic photophysical properties for nanoimprinted P3HT gratings. Due to chain orientation in nanoimprinted P3HT structures, the pattern exhibit difference in absorption spectra when excited by light with different polarizations. In Figure 20, solid lines are absorption spectra of P3HT gratings when the incident light is polarized perpendicular (90^o) to grating lines, while red dashed lines correspond to the case when the incident light is polarized parallel (0^o)

to the grating lines. The difference in the absorption spectra between two incident polarizations is contributed to chain ordering in nanoimprinted P3HT gratings. The close similarity of the absorption spectra for the first (Figure 20(a)) and the second (Figure 20(b)) nanoimprints corroborates the conclusion that subsequent exposure to heating in step-and-repeat thermal nanoimprint has no impact on chain configuration, hence pattern stability. To find out the temperature stability of the nanoimprinted P3HT gratings, additional heating on hot plates at 120^{o}C for 10 hours and 180^{o}C for 30 mins showed no sign of pattern reflow or decay. This behavior is drastically different from amorphous polymers such as poly(methyl methacrylate) and polystyrene. Numerous studies have shown that significant pattern reflow or decay occurred when nanoimprinted structures were annealed at a temperature close to or slightly above the polymer T_g [60]. Although it is found that polymer chains are also stretched in amorphous polymers after nanoimprinting, the stretched and aligned chain configuration is not stable because of weak interchain interaction. Instead, the residue stress in amorphous polymer structures patterned by thermal nanoimprint due to chain stretching often contributes to pattern reflow, even at temperatures below T_g, because chain ordering is not thermodynamically favored state for amorphous polymers. Thus, the ability to maintain stable structure through enhanced interchain interaction in stretched semicrystalline polymer is the key enabling factor for step-and-repeat solid-phase thermal nanoimprint. Structural stability is even more critical for device applications because the patterned functional polymer structures are usually permanent

components in devices and long-term stability is important to device performance stability.

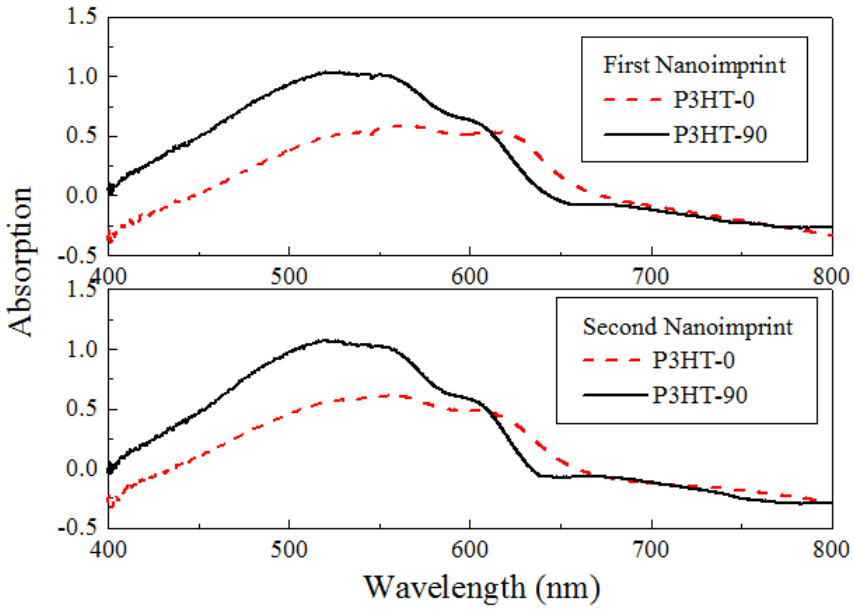

Figure 20. Polarized absorption spectra of P3HT gratings formed in the first and the second nanoimprints.

3.3.3 Double nanoimprint

Figure 21 shows a two-step imprinted image of the P3HT. In the first step, the P3HT was imprinted at 170^{o}C by the 350nm grating mold. In the second step, the sample was rotated by 90 ° and the grating patterned in the first step is imprinted again with the same mold at 150^{o}C under 5 MPa for 5 min. Through this double nanoimprint on the same area we obtain square pillars in P3HT substrate. As clearly shown in the Figure 21, the grating lines patterned in the first nanoimprint is not destroyed by the second

nanoimprint. This result is related to the thermal stability of P3HT. The stability of the P3HT grating pattern exhibited in double nanoimprint provides additional evidence that step-and-repeat thermal imprinting is highly plausible.

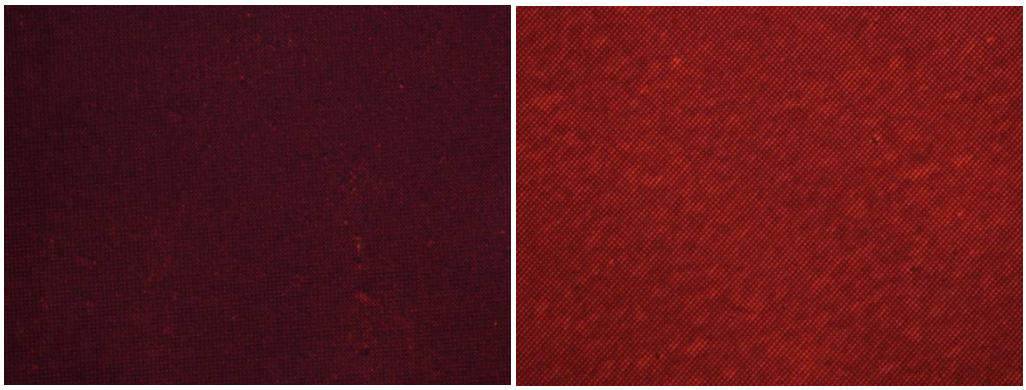

Figure 21. Polarizing optical microscope images of P3HT gratings after double nanoimprint. The angles between the grating lines and the incident light polarization direction are 0^{o} and 45^{o} in dark and bright images respectively.

Figure 22 shows the SEM images of the double-nanoimprinted pillars inP3HT and in polystyrene. In both cases, grid patterns after the second nanoimprint are clearly seen. The edge of the P3HT pattern didn't melt or fall down. But in the polystyrene case, an additional heat leads to the edge sinking due to polymer flow.

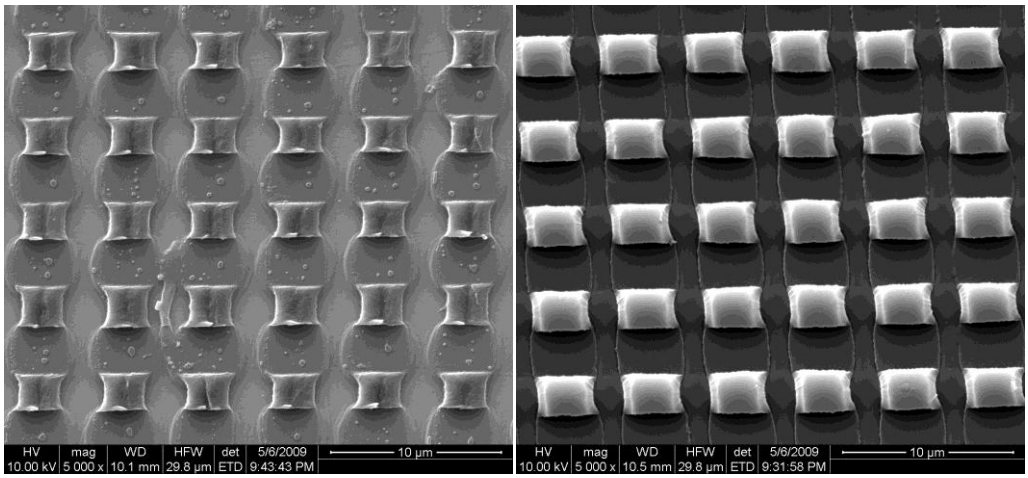

Figure 22. SEM image of double-nanoimprinted P3HT and polystyrene.

Despite of its simplicity, solid-phase step-and-repeat nanoimprint is expected to bring forth several breakthroughs in thermal nanoimprint. The biggest advantage is the throughput enhancement. Traditional thermal nanoimprint of amorphous polymers requires cooling to a temperature significantly below T_g for demolding. The heating and cooling cycles greatly increase overall process time and reduce throughput. With solid-phase nanoimprint, the mold and substrate assembly can be kept at constant processing temperature and repetitive nanoimprints can be performed without heating and cooling cycles. In a typical thermal nanoimprint, the pattern formation is usually less than a few seconds while the heating and cooling cycle is around 10 to 20 minutes, depending on tool setup. Removing heating and cooling cycles immediately improves the throughput of thermal nanoimprint by at least 100 times.

The second major advantage of the step-and-repeat solid-phase nanoimprint is the ability to pattern large substrates with smaller molds. Consecutive nanoimprint on

the same substrate is not possible in conventional thermal nanoimprint because subsequent heating to well-above T_g destroys pattern formed in preceding nanoimprints. Tool modification and careful thermal management, which is not an easy task, must be carried out to enable step-and-repeat process for thermal nanoimprint [61]. The solid-phase nanoimprint presented here requires no special handlings. Roll-to-roll nanoimprint is currently mostly implemented with UV-curable nanoimprint for high-throughput nanopatterning [62]. It is very difficult to achieve roll-to-roll thermal nanoimprint because accurate temperature zoning and precise heat management are imperative to avoid pattern reflow. However, solid-phase nanoimprint is fully compatible with the roll-to-roll scheme and can be implemented at a similar level of complexity as UV roll-to-roll nanoimprint for nanopatterning with exceptionally high throughput.

3.4 Summary

In summary, we present solid-phase step-and-repeat nanoimprint based on stress-induced yielding in semicryalline polymers. P3HT gratings were patterned by nanoimprint below the T_g and T_m with typical pressure for thermal nanoimprint. Solid-phase nanoimprint at the highest tolerable temperature for preserving pattern integrity can significantly reduces the pressure needed for pattern formation. The ability to perform nanoimprint in a step-and-repeat fashion is due to the structural stability enhanced by chain stretching and alignment in semicrystalline polymers. Most functional polymers, including but not limited to, conductive, semiconducting,

piezoelectric, and biofunctional polymers are thermoplastic semicrystalline polymers. Solid-phase nanoimprint not only provides a simple and non-destructive patterning technique for those polymers, but also presents the ability to fine-tune material properties though chain stretching and alignment. Solid-phase nanoimprint is expected to become the ideal technique for patterning those functional polymers for flexible and large-area electronic, photonic and bioengineering devices and systems. Many engineering plastics are also semicrystalline polymers. Thus, it is possible to use solid-phase nanoimprint to create stable surface nanostructures to render superhydrophobic and anti-reflection properties in polymer films or sheets for a wide range of applications. With its compatibility with step-and-repeat process and roll-to-roll scheme, solid-phase nanoimprint has the potential to open a new chapter for thermal nanoimprint in industrial-scale nanomanufacturing.

Nanoimprint patterning of semicrystalline polymers below their melting temperatures can be achieved based on the principles of stress-induced yielding. Such solid-phase thermal nanoimprint is fully compatible with step-and-repeat and roll-to-roll schemes for high-throughput nanopatterning over large substrate surfaces. Coupled with its ability in controlling chain orientation and crystallization, solid-phase thermal nanoimprint is expected to have far-reaching impact on functional polymer patterning.

CHAPTER IV

A RAMAN SPECTROSCOPIC STUDY OF POLYMER CHAIN CONFORMATION AFTER NANOIMPRINT

The polymer thin films after nanoimprint often show two-dimensional (2D) orientation depending on the conditions of sample preparation. The final polymer chain orientation originates from multiple factors including flow-induced chain alignment, polymer chain conforming to mold surface and polymer crystallization in micro- and nanostructures. In this work, the Raman scattering from nanoimprinted oriented samples of poly(methyl methacrylate) (PMMA) were studied by polarized Raman spectroscopy in which the incident laser light was coupled into the patterned polymer thinfilm. The Raman analysis opens a route for fine-tuning polymer properties by nanoimprint since the physical properties of polymers are usually affected by their chain configuration.

4.1 Introduction

Nanoimprint lithography is known as an economical and high-throughput nanopatterning technology for the production of nanostructure [63]. It can be used in fabricating nano-scale patterns as small as 5nm [64]. This technique has wide variety applications such as organic photovoltaic device [65], organic transistors [47] and transparent electrode [66]. During nanoimprint, the polymer is forced to flow under pressure, it leads to the direction and the extents of chain orientation depend on the

flow pattern of polymer melt. In thermal nanoimprint, the polymer flow distribution is affected by many nanoimprint parameters, such as mold pattern size, shape, density and height, polymer film thickness, nanoimprint temperature, processing time, and polymer molecular weight. These conditions directly influence flow behavior, which determines the accuracy of the final geometry of imprinted nanostructures. The actual chain orientation of molecular groups in polymer micro- and nanostructures are complicated, but it is crucial for understanding the chemical properties and controlling the physical properties.

Mechanical property of a polymer is an important factor to choose process conditions in nanoimprint lithography. There are a few simulation and studies focusing on the flow behaviors of thin polymer films [67]. These observations of polymer flow during nanoimprint process suggest a mode of deformation where polymer adjacent to the master sidewall has enhanced flow properties and deforms in separate peaks upward and adjacent to the master sidewall [68]. However, the polymer deformation and the optical effect have not clearly been revealed because of the difficulties of evaluation in resist time evolution process. To obtain the temperature and time evolution of polymer profiles experimentally, Raman spectroscopy is potentially an especially efficient tool, providing quantitative information both about intermediate and reaction products and about reaction kinetics [69]. Purvis et al [70] suggest that the changes of the Raman tensors observed for polymer thinfilm may be due to conformational changes. Orienting at different temperatures may produce samples with a different distribution of conformers for a given birefringence. With

orientation averaging for a partially oriented sample, it has been possible to determine which molecular Raman polarizing components contribute to the spectra [71] and which processing conditions lead to the change in the birefringence effect, and then to infer information about the conformation of the polymer in nanoimprint process. So that a general understanding of the processing conditions on the birefringence can be obtained by the Raman study. Such knowledge can help answer fundamental questions about the processing conditions, which is ubiquitous and critical for the natural and physical functions of polymer. The understanding of the growth process and the distribution of orientations of the structural units of polymers can also help us to recognize the interactions in the modified conditions and provide a general technique in optimizing the process conditions.

In this study, PMMA was used to investigate the polymer chain conformation after nanoimprint. PMMA is an amorphous polymer, which can be easily nanoimprinted at different processing conditions. This simplifies the experimental arrangements in obtaining samples and makes it easier to study the birefringence caused by different processing conditions. The details of nanoimprinted structure can be investigated by Raman spectroscopy (Raman), the difference of sample orientation can be analyzed from the classical interpretation of depolarization ratios (from which bands are assigned to symmetrical and nonsymmetrical species). Many reports about the distribution of the molecular orientation have been obtained from measurements with Raman spectroscopy [71, 72]. In those studies, the purpose was to analyze the molecular components in the interface region in more detail by micro Raman spectral

measurements. Our interest mainly focuses on the cross relationships in the birefringence of oriented PMMA and nanoimprint conditions for both fundamental and applied purposes. Thus, the method in this work is presented to determine orientation in a patterned film from polarized Raman measurements obtained by using different conditions, such as nanoimprint temperature, processing time, mold size and molecular weight. By the Raman spectroscopy study, it is possible to understand the deformation process of polymer in nanoimprint lithography and obtain fairly detailed information about the distribution of orientations of the structural units in an oriented solid polymer.

Raman spectroscopy offer several advantages in investigating polymer chain orientation of the patterned polymer, both for the determination of the molecular composition of materials and for obtaining structural information by molecular vibration analysis [73]. Additional information about symmetries can be extracted because the patterned polymer orientation can be controlled, this is important in the case of Raman depolarization ratios since to determine these ratios accurately the polymer chains must be distributed isotropically [71].

This work is the first quantitative effort that combines a broad spectrum of nanoimprint temperature scales in a single analysis. According to the previous studies, the variations in embossing tool geometry and polymer film thickness during viscous flow distinguish different flow driving mechanisms [35]. That may be responsible for Raman polarization ratio. With the right-angle Raman scatting geometry used, correlations between the direction of the incident polarization laser beam,

nanoimprinted gratings direction and the observed Raman band intensities have been used to specify the orientation of the polymer backbone and pendant groups. Because the depolarized groups of oriented Poly(methyl methacrylate) (PMMA) are quite stable, which enable us to compare the distribution and intensity of molecular orientation and predicted the effect of the birefringence of the samples on different processing conditions.

4.2 Experiment

Poly(methyl methacrylate) (PMMA) solution in toluene (5 wt %) was spin-coated on 100 nm thickness silver on Si wafer to achieve a thin film. Si grating mold with 700 nm, 10μm, 20μm period and 50% duty cycle was used to achieve the designed patterns. These mold was coated with 1H,1H,2H,2H-perfluorodecyltrichlorosilane (FDTS) for easy mold releasing after nanoimprint. The nanoimprint was carried out at 120^{o}C, 150^{o}C and 180^{o}C, with a pressure of 50 kN/cm^{2}. Polarized Raman spectra were recorded with 633 nm HeNe laser; wihich has a power of about 15mW. The focus beam was around 5μm in diameter.

In the Raman spectrum testing, the 0^{o} polarized laser as a parallel beam was vertically injected into the 50x magnification objective microscope lens and onto the patterned PMMA samples, Raman photons were collected by the same objective, passed through a polarizing analyzer, and detected by a cooled, charge-coupled device detector. The width of the laser beam was limited to 5μm. The specimen was rotated to make sure the patterned cavity direction is parallel to the incident laser light. Tests

were carried out to ensure that no measurable scattered light was collected from the surroundings. The perpendicular polarized Raman intensities were measured by maintaining polarized laser beam and rotating the samples with 90^{o}C.

4.3 Results and discussion

In nanoimprint lithography, a polymer thinfilm suffers large deformation from a mechanical stress and polymer flow. The mold patterns, initial thickness of the polymer and nanoimprint conditions affect on the deformation of polymer. Thus, understanding the polymer deformation process is extremely useful to design optimum process conditions and material characteristics. As the structures become smaller, the behavior of the thin polymer film becomes complex. The cross-sectional profile of the deformed polymer is very useful to provide the resolution and the quality of imprint lithography.

The Raman spectra of PMMA gratings of 15k and 75k molecular weight after nanoimprinting at 180^{o}C, with the thickness around 200nm, 600nm are shown in Figure 22(a) and (b). We can find there are slightly different in the relative intensities of the Raman bands. So in the following experiments, the PMMA thin film thickness will be kept as 200nm to investigate the Raman spectrum.

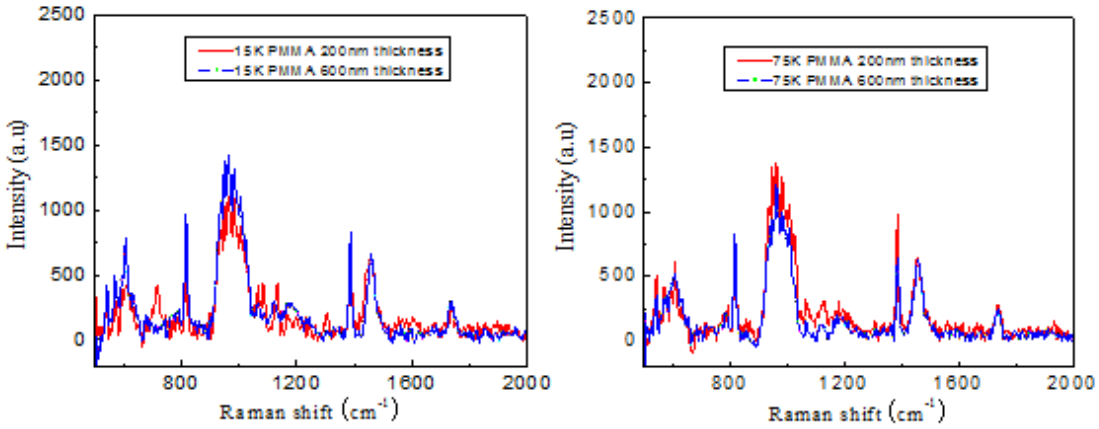

(a) (b)

Figure 23. Raman spectra of 15k, 75k PMMA (no gratings) with different thin film thickness.

4.3.1 Raman spectroscope of PMMA

Since PMMA has an unsymmetrical repeat unit and the sample examined was amorphous it is reasonable to expect the molecule to exist in a number of conformational states [63]. In this study, Micro Raman spectra were recorded in the region between 500 and 2000 cm^{-1}. In this region, for PMMA, all strong Raman peaks occur on side groups: polarized symmetric stretching mode of C-C-O bond (604cm^{-1}); strongly polarized symmetric stretching mode of C-O-C bond (818cm^{-1}), the infra-red bands at 991 cm^{-1} arises from CH_3-O, depolarized asymmetric stretching mode of C-H bond (1456cm^{-1}) in α-CH_3, polarized stretching mode of C=O bond (1736cm^{-1}) and depolarized rocking mode of a-CH_3 bond (970cm^{-1}). The skeletal C-C mode is very

week in PMMA Raman signal, thus Raman spectroscopy cannot evaluate the ordering of PMMA main chain, the diagram shown on Figure 24.

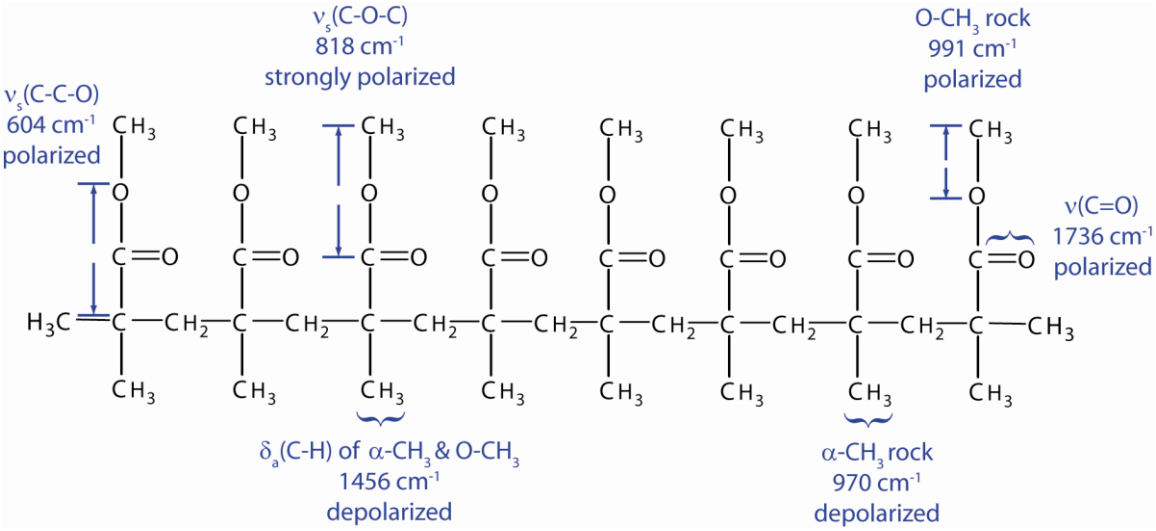

Figure 24. Raman spectroscope of PMMA.

4.3.2 Birefringence of nanoimprinted PMMA

In PMMA gratings patterned by nanoimprint, the polymer chains will be stretched and aligned in the direction perpendicular to the grating ridges and trenches, which leads to optical birefringence in the directions perpendicular and parallel to the grating lines. The optical birefringence can be directly observed in polarizing microscope with crossed polarizes. When the incident light is polarized parallel or perpendicular to the chain stretching direction, the polarization state of the incident light will be unaffected. After exciting the PMMA film, the polarized light will be completely blocked by the top polarizer, leading to a dark image of the sample. When

the PMMA grating is rotated by an angle, the incident polarized light will see the optical birefringence in the film. The birefringence will rotate the polarization direction of the incident light. After propagating inside the film, the incident light will develop a net component along the polarization direction of the top polarizer, leading to a bright image of the sample. The pictures of 15k, 75k molecular weight PMMA grating nanoimprinted on the glass at 180^{o}C, 5mins, in polarizing microscope with crosses polarizer were shown in Figure 25. Polarized transmission spectra of 350nm patterned films, shown in Figure 26 also reveal the patterned film orientation after nanoimprint.

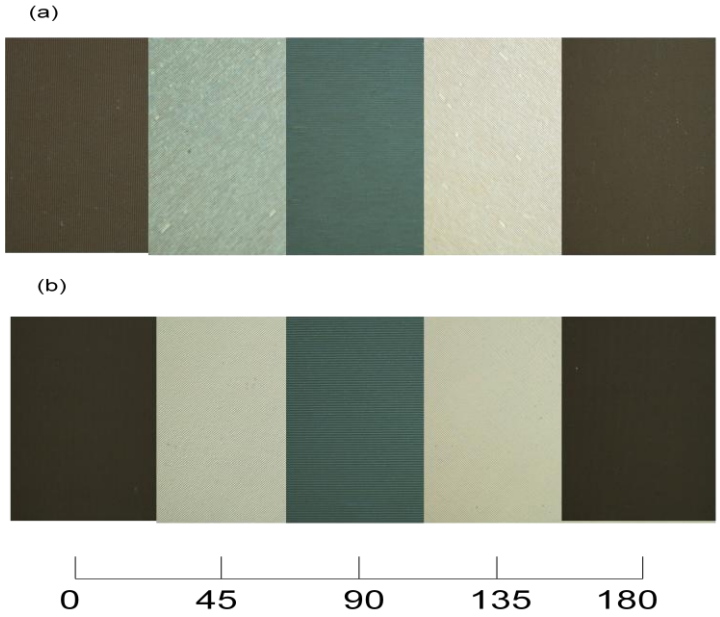

Figure 25. PMMA grating nanoimprinted at 180^{o}C, 5mins, in polarizing microscope with crosses polarizer, a)15k PMMA, b) 75K PMMA.

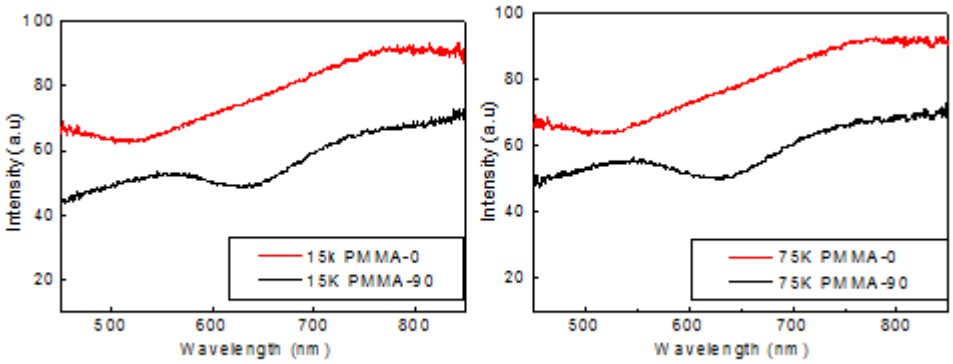

Figure 26. Polarized transmission spectra of PMMA. Dark: The incident light is polarized perpendicular to grating lines, red: parallel to grating lines, a) 15K, b) 75K.

4.3.3 A schematic of PMMA flow

In the nanoimprint process, as the mold is pushed into the polymer film, the polymer flows along the mold surface as shown in Figure 27. The polymer film begins to be compressed and extruded from the bottom of the pattern. Shear deformation is most happened near the stamp surface and corner, the polymer is then forced s to move along the sidewall of the mode due to the friction force, thus it flows upwardly and fills the cavity of the mold. At the end of the imprint process, the polymer film under the mold is heavily compressed and majority of the polymer is pushed from the original position to the horizontal cavity. Due to the compression of the polymer film, high density areas are concentrated under the stamp pattern and, as a result, a large stress is generated at the polymer surface and manifestly birefringence effect also arises in this region. In nanoimprint process, process parameters, such as polymer thickness, process time, temperature and cavity size, are responsible for the

deformation of the polymer. Chain orientation due to polymer deformation will lead to the intensity change in the Raman peaks.

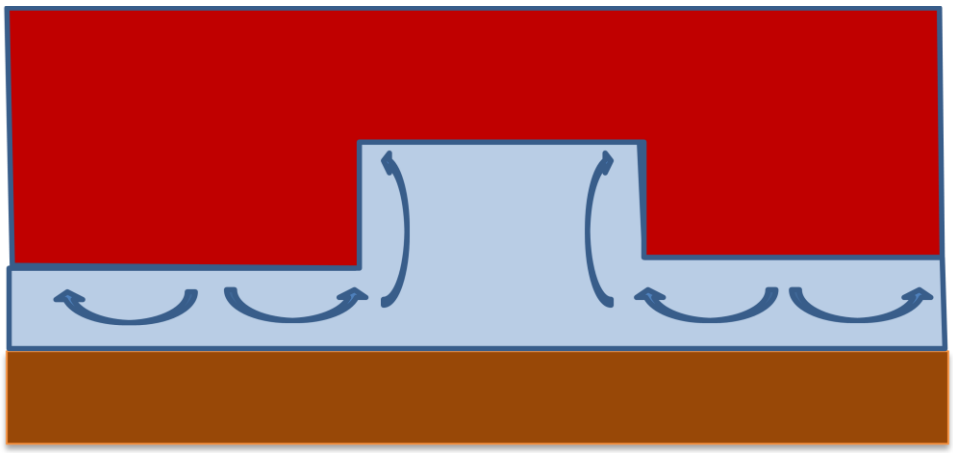

Figure 27. Polymer flow during nanoimprint process.

4.3.4 Raman spectra of PMMA samples

Figure 28 is the first quantitative effort that combines a broad spectrum of nanoimprint temperature scales in a single analysis. Stress non-uniformity arising from flow inhomogeneity. At the lower temperature, the polymer on the substrate suffers more stress arises from the long range contact mechanics of the stamp. At the higher temperature, the polymer flow has more impact on the birefringence effect. The measurement of the Raman spectrum of samples nanoimprinted at different temperature was directly compared with the combined strain accommodation and the polymer flow effect. Although certain limitations of the analysis were noted, the ability to suppress the effect of temperature influence was strongly suggested. Figure 29 shows the

birefringence influences on the PMMA nanoimprinted at different temperature, it is important evidence.

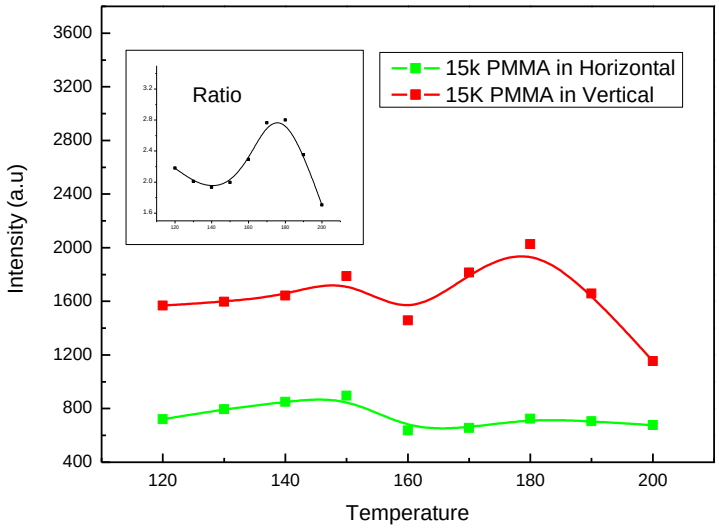

Figure 28. Raman spectrum of PMMA at different temperature.

During the nanoimprint process, compressive stresses generated under the mold pattern due to the compression of the polymer film have significant effect on the polymer viscoelastic behavior, and force the polymer to flow and to fill the cavity of the stamp. At a relatively lower temperature, a larger stress is on the shear side of the polymer film induced by the contact between the film and cavity of the mold, which causes the mechanical stress on the film. Polymer polarization effect was enhanced near the cavity sidewalls due to stress concentration and/or shear thinning. These produced a large difference in viscosity between the polymer near the master sidewall

and the polymer in central regions of the mold, which leads to the amplified ratio of the two peaks at 813 and 990 cm^{-1}.

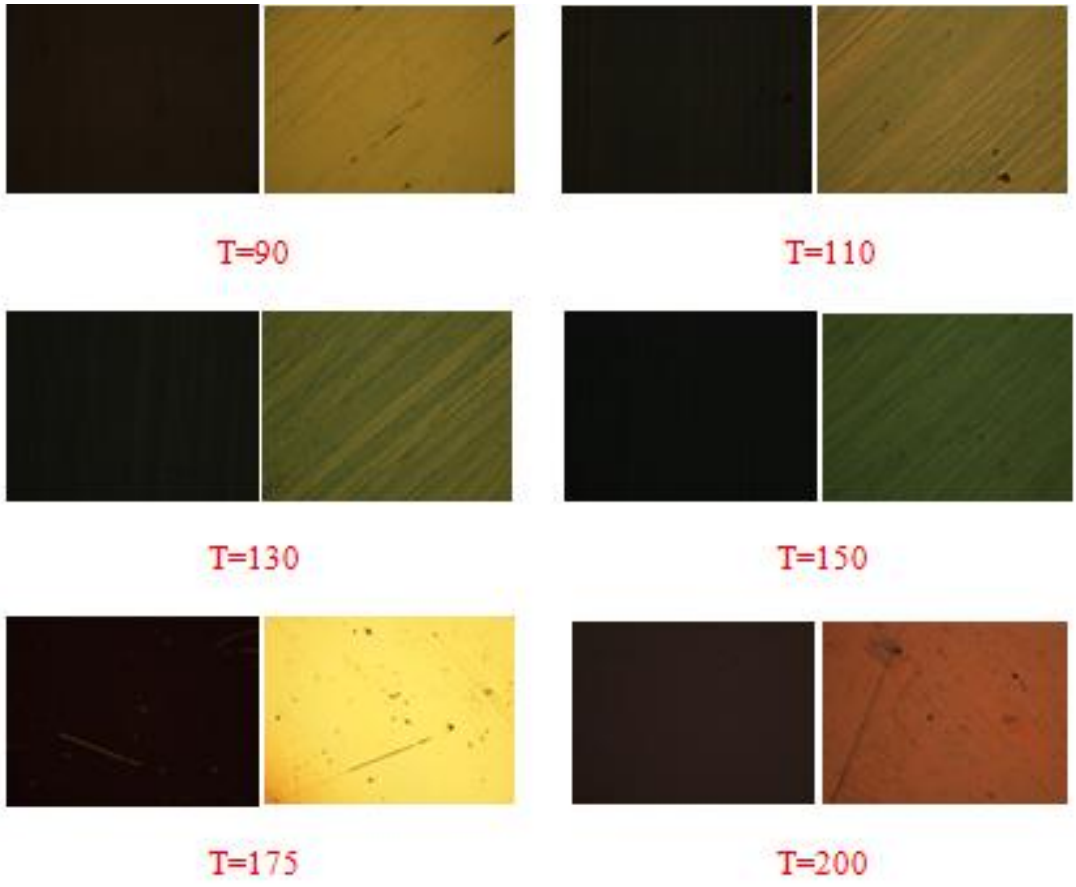

Figure 29. Polarizing microscope images of P3HT gratings patterned by nanoimprint at different temperature.

Stress non-uniformity arising from flow inhomogeneity. At the lower temperature, the polymer on the substrate suffers more stress associated with the long range contact mechanics of the stamp. At higher temperature, the polymer flow has more

effect on the birefringence effect. A measure of the Raman spectrum of samples nanoimprinted at different temperature was directly compared with the combined strain accommodation and the polymer flow effect. Although certain limitations of the analysis were noted, the ability to suppress the effect of temperature influence was strongly suggested. Figure 30 shows the birefringence effect of PMMA nanoimprinted at different temperature, it is evidence.

The Raman spectra with different nanoimprint time at the same temperature are shown in Figure 28. On the patterns, where stress relaxation mechanisms are accelerated with the longer printing time, the viscous flow mechanisms will slowly decrease. The relaxation of the induced stresses for longer processing time is manifested as a change of the strong Raman peaks corresponding to PMMA side groups. It is expected that relative recovery would be greater for longer processing time at higher temperature. This is also supported by experimental results in Figure 30. For 5 min, 30 min, and 60 min of nanoimprint, change in polymer deformation at 120 ℃ was very small, that means for the case of process temperature at relatively lower temperature, final polymer deformation was almost the same as maximum deformation in the process.

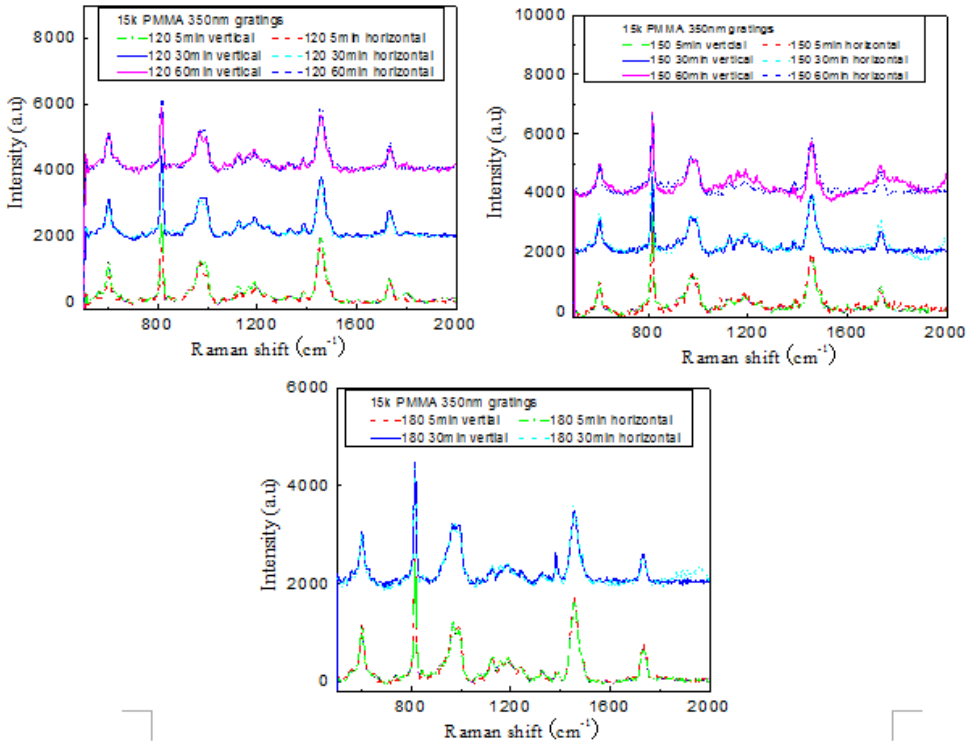

Figure 30. Raman spectra of 15k PMMA samples, nanoimprinted at different temperature and time.

Higher molecular weight PMMA has a significantly larger viscosity during the imprint process. This generates greater stress on the surface as the viscous material flowed into the mold cavity. The Raman spectra of 75k PMMA nanoimprinted at 150^{o}C with different processing times are shown in Figure 31. Compared to the 15k PMMA, it is found that higher molecular weight sample exhibits greater polarization ratio. This observation is due to the fact that the side chain of the higher molecular weight polymer has the potential to orient in the direction of material flow or parallel to the surface.

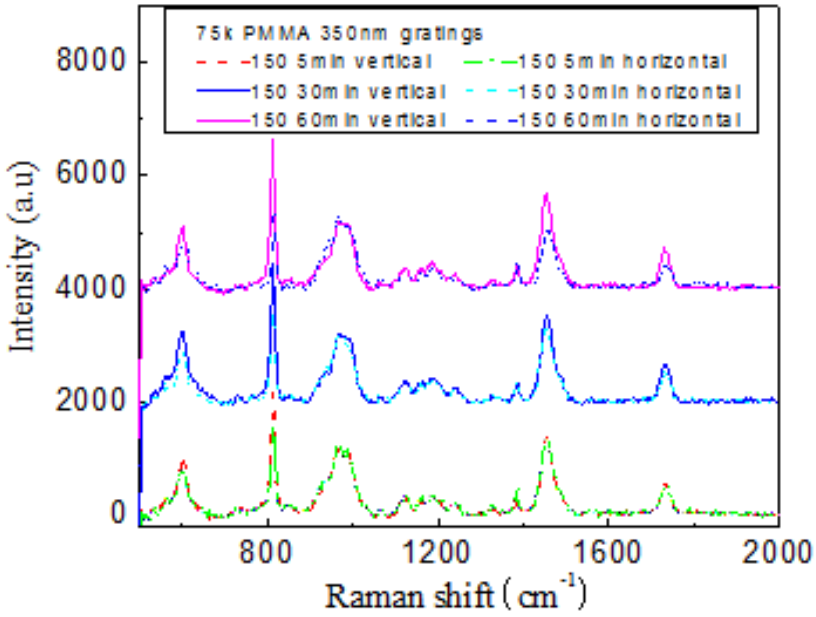

Figure 31. Raman spectra of 75k PMMA samples, nanoimprinted at 150 ^{o}C.

Figure 32 showed experimental results of process temperature at 150 and 180^{o}C. The Si grating mold is a grating with 10um period and 50% duty cycle. In comparison with the results showed above, we find more changes of Raman peak happened on the unpatterned area and the polarized Raman peak decreases on the patterned area. From the Figure 32a, the Raman peak at 813cm^{-1} on the gratings decreases in comparison with the original PMMA thin film and almost disappears in the vertical direction. One of the possible reasons is the polymer flow might be limited near the edges of the mold and it is bunched up near the mold edges. In the nanoimprint process, as the grating size increases to 5μm, majority of polymer is pushed over larger distances than in 350nm gratings. In this process, the polymer near the cavity is pushed towards the sidewall and the polymer under the cavity is escalated

and compressed. Therefore resulting in a Raman peak change happens near the sidewall and a large stress and change in peak intensity in the patterned region, which is sufficient to verify the polymer orientation. In the case of 5 μm gratings patterned at 120°C, the changes in Raman peak is very small, that means the viscous force is significantly greater than surface tension forces in large size gratings.

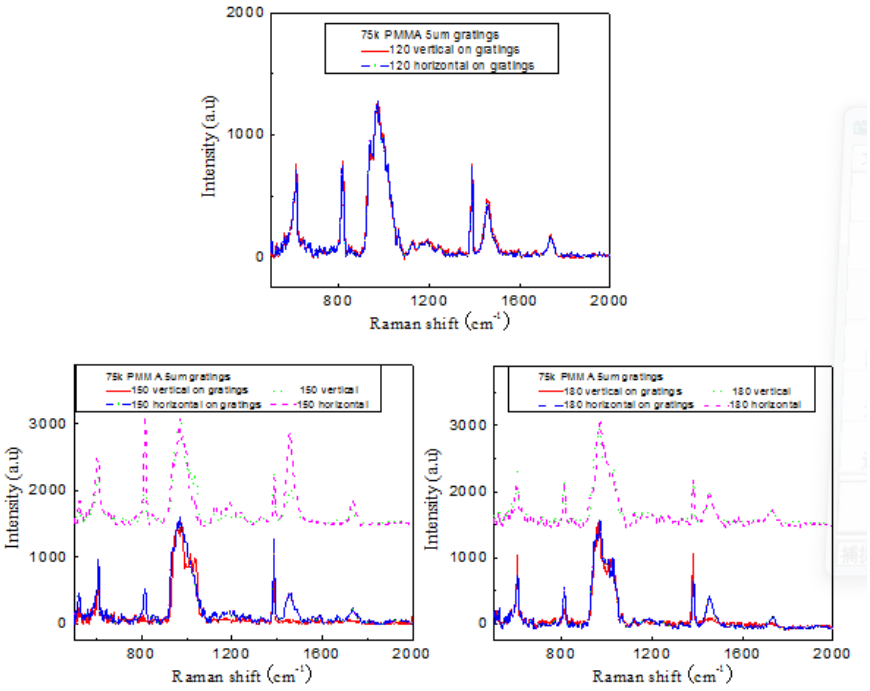

Figure 32. Raman spectra of 75k PMMA samples, nanoimprinted at 120,150, 180°C, the mold cavities are 5 μm.

4.4 Conclusion

In summary, the changes of PMMA Raman spectrum are studied for various imprinting conditions such as nanoimprinting time, temperature, and the cavity size of

mold pattern. At the lower temperature, the polymer on the substrate suffers more stress arises from the long range contact mechanics of the stamp. At the higher temperature, the polymer flow has more impact on the birefringence effect. Because polymer properties depend on chain conformation, nanoimprint opens up an easy route toward manipulating polymer properties in addition to polymer patterning.

CHAPTER V

INCREASE CARRIER MOBILITY IN POLYMER THIN-FILM TRANSISTORS THROUGH STRETCHED-INDUCED CHAIN ORIENTATION

In this work, semicrystalline poly(3-decylthiophene-2,5-diyl) (P3DT) thin film was stretched by a facile technique. Polarizing microscope images show the stretched film has strong optical birefringence, which is a consequence of chain extension and orientation in the amorphous region. A blue shift of peak absorption spectrum and the lowering of the scattering angle in the X-ray diffraction pattern indicate that the unraveling of the polymer chains in the crystalline domain also occurred. Organic thin-film transistors (OTFTs) based on the stretched P3DT film showed a significant increase in hole mobility. For OTFTs with channel aligned parallel to the stretching direction, the mobility is increased by 20 times as compared to the un-stretched P3DT. This ratio of hole mobility between the parallel and the perpendicular directions is about 4. These results indicate that stretching is an effective technique for improving the performance of organic devices based on conjugated polymers.

5.1 Introduction

In recent years, organic thin-film transistors (OTFT) have drawn great attention for their potential applications in low-cost flexible electronics and sensors.[74] Particularly, polymer-based OTFTs have processing advantages because the devices

and circuits can be fabricated with solution processing, which eliminates the need for the slow and expensive vacuum processing in their fabrication. Currently, the application of OTFT is limited by the device's low performance. There are many ways to improve the performance of an OTFT, and one of the critical issues remains to be the material properties, such as carrier mobility. Polymer semiconductors suffer low mobility due to disordering in conjugated polymer thin film, thus the techniques for improving carrier mobility focus on improving chain ordering in polymer semiconductor thin film.

It is well-known that, in conjugated polymer films, the processing history, such as solvent type, solution concentration, thermal annealing, and substrate surface rubbing, has significant impact on polymer chain morphology.[75] The formation of highly ordered chain packing in polymer materials is desirable because the physical properties (e.g. mechanical strength and electrical conductivity) of oriented polymers are often much higher than those of amorphous materials.[76] Since the electrical and photophysical properties of conjugated polymers are highly dependent on film morphology and polymer chain configuration, many techniques have been developed to introduce ordered packing of polymer chains, such as synthesizing regioregular polythiophenes,[77] enhancing crystallization by liquid crystals,[30] chain orientation by nanocomfinement,[78] self-assembly,[31] substrate texturing or rubbing,[79] surface chemical treatment,[80] tensile drawing,[81] and gel processing in polyethylene.[82]

Among all techniques that can achieve chain orientation, stretching is the simplest one. Optical property changes in stretched conjugated polymers have been

reported. [11-12]. In this work, the electrical transport property of a stretched polythiophene was studied and presented. Chain ordering was achieved through a facile and effective tape-assisted stretching method, and several analytical techniques were used to characterize the chain ordering in the processed thin film. OTFTs based on the oriented conjugated polymer thin film were fabricated. The characterization results indicate chain orientation by stretching can significantly increase the carrier mobility, making stretching orientation a practical technique for improving the performance of organic electronics.

5.2 Experimental details

Polythiophenes, such as regioregular poly(3-hexylthiophene) (P3HT), are commonly used for OTFTs because of their high mobility. Instead of P3HT, poly(3-decylthiophene-2,5-diyl) (P3DT) (Figure 33(a)) is used in this work because it has very low yield strength at room temperature. Although the carrier mobility for P3DT is much lower than that for P3HT due to lower crystallinity and bulkier side groups, the easy processing allows P3DT to be stretched at room temperature to study the impact of chain orientation. In practical applications, other conjugated polymers can be stretched by nanoimprinting at elevated temperatures because nanoimprint can induce chain orientation through forced melt flow.[83]

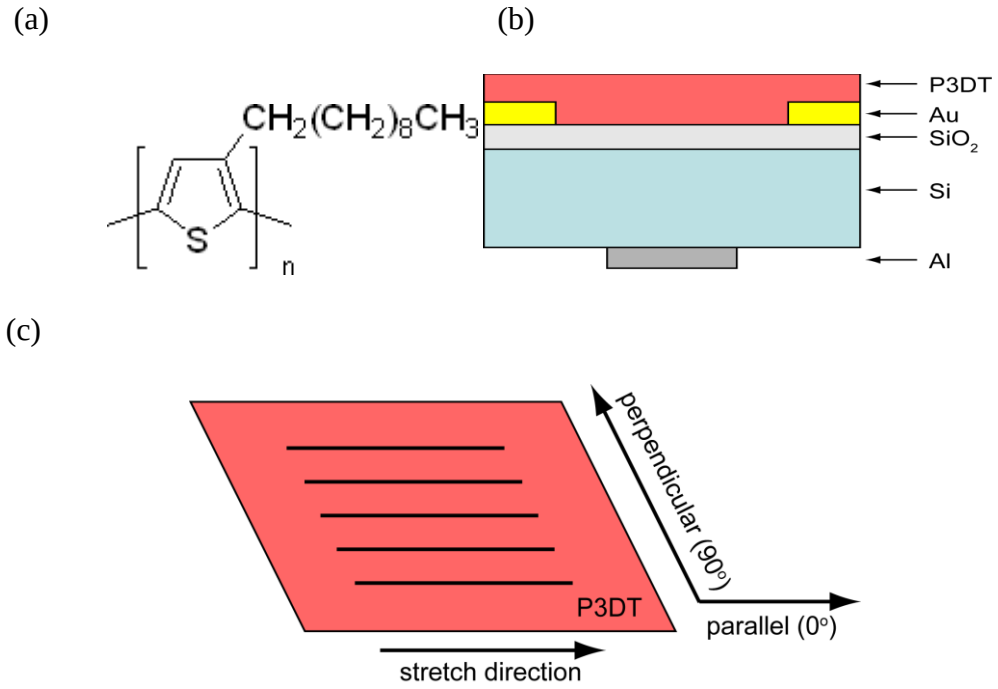

Figure 33. (a) Molecular structure of P3DT; (b) Cross-sectional view of the OTFT device based on stretched P3DT; (c) The term "parallel" refers to the direction along the stretch direction (0^o angle), and the term "perpendicular" refers to the direction perpendicular to the stretch direction (90^o angle).

Regioregular P3DT was purchased from Sigma-Aldrich and dissolved in dichlorobenzene (25mg/ml). The solution was used to spin-coat a P3DT thin film on a silicon wafer. After spin-coating, the thin film was annealed at 110^oC for 5 minutes. On another silicon wafer, an oxide layer of 100 nm thick was thermally grown. The source and drain electrodes for the OTFTs were patterned by a sequence of steps

including photolithography, metal evaporation and lift off. The source and drain contacts consists of 5 nm titanium and 100 nm gold. The width/length (W/L) ratio for the OTFTs is 3000. After the patterning of the source/drain electrodes, one end of the P3DT film was fixed and the other end was picked up by a sticky tape and the film was mechanical stretched to twice of its original length by pulling the tape. The stretched film was then transferred to the top of the substrate that has the source/drain contacts. In order to improve the contact with the electrodes, and enhance the adhesion to the SiO_2, the stretched thin film was pressed against the substrate with a flat silicon wafer at room temperature at 2×10^6 Pa for 5 minutes by a mechanical press. After those steps, a bottom contact OTFT with stretch-oriented P3DT thin film as its channel region was completed, as shown in Figure 33(b). To compare the carrier mobility anisotropy parallel and perpendicular to the stretch direction, two OTFTs were fabricated. In the first device, the stretching direction was aligned parallel to the longitudinal direction of the channel, while it was aligned perpendicular in the second device. As shown in Figure 33(c), in all characterizations, the term "parallel" refers to the direction along the stretching direction, which has a 0^o angle with the stretch direction. The term "perpendicular" refers to the direction that forms a 90^o angle with the stretch direction.

The stretched P3DT film was characterized through polarized absorption spectra taken from a spectrometer (Ocean Optics USB2000) coupled to a polarizing microscope (Nikon Eclipse LV100POL) with optical fibers. Optical birefringence in the stretch-oriented P3DT thin film was directly visualized in the Nikon polarizing

microscope with crossed polarizers. The packing of the polymer chains before and after stretching was probed by X-ray diffraction (Bruker D8 Discover). The current-voltage (I-V) characteristics of the fabricated OTFTs were measured by HP 4200 semiconductor analyzer. Device parameters, such as carrier mobility, were extracted from the I-V curves in the linear region.

5.3 Results and discussion

Regioregular P3DT is semicrystalline and its thin film consists of both crystalline domain and amorphous region. The overall properties exhibited by the semicrystalline thin film are the average of the contributions from both regions. Due to the stretching, there are two changes that can occur in chain conformation. At the beginning of the stretching, the extension of the film is accomplished by the sliding of the main chain in the amorphous region along the stretching direction because polymer chains in the amorphous region have weaker inter-chain interaction. Polymer chains extend and acquire a macroscopic orientation, resulting in strong optical birefringence in the stretched thin film. If the P3DT thin film continues to be stretched to a large strain ratio, the extending and sliding of the chains in the amorphous region alone are not enough to accommodate the large strain, and the unraveling of the polymer chains in the crystalline domain ensures when the amorphous region is stretched to its maximum extension. The unraveling of the crystalline domain impacts its electronic structures, consequently the electrical and photophysical properties of the stretched film.

5.3.1 Polarized image of Stretched P3DT film

P3DT thin film before stretching showed no optical birefringence when it was placed between two crossed polarizers in a polarizing microscope. This is because the small crystalline domains randomly distribute in the amorphous regions and yield an optically isotropic film. After stretching, the incurred chain orientation gave rise to variable transmission when the thin film was rotated to misalign the stretching direction and the directions of the crossed polarizers, as shown in Figure 34. When the stretching direction was aligned parallel to the incident light polarizer (0^o), the transmission was very low because all light was blocked by the top polarizer, which was aligned perpendicularly to the incident polarization. When the stretched thin film was rotated, the polarization direction of the incident light can be rotated due to the optical birefringence in the stretched P3DT film, thus some of the light escaped from the top polarizer.[84] The brightest field was reached when the P3DT film was rotated by 45^o. After that, the transmission gradually decreased and reached the minimum again when the thin film was rotated by 90^o.

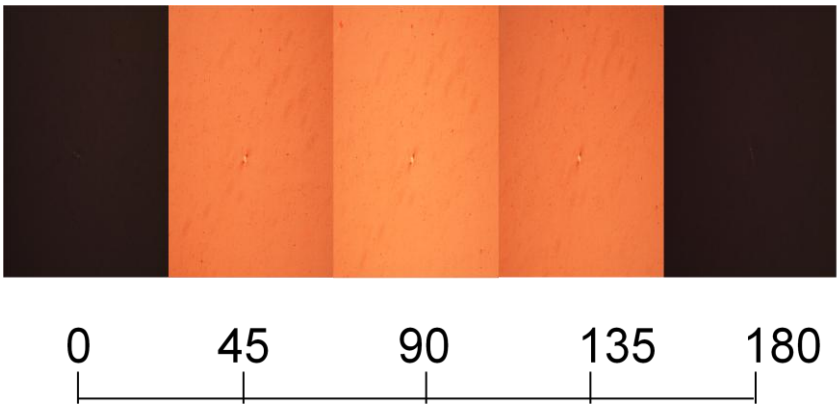

Figure 34. Polarizing microscope images of the stretched P3DT thin film between two crossed polarizers. The angle below the images refers to the angle between the stretch direction and the bottom polarizer (incident light).

5.3.2 Absorption spectra of stretched P3DT

The chain orientation in the stretched thin film also yields a change in the polarized absorption spectra. The absorption spectra of the stretched P3DT thin film with the incident light polarized at the parallel and perpendicular directions were shown in Figure 35. In addition to the observation of absorption dependency (dichroism) on the polarization states, the absorption peaks for the parallel (573 nm) and the perpendicular (500 nm) directions were different. The absorption spectra for the original P3DT film showed no dichroic effect, and it was also plotted in Figure 35 for comparison. The blue shift of the peak absorption wavelength in the stretched P3DT film indicates an increase in the HOMO-LUMO gap. It is known that conjugated polymers in the amorphous state have larger HOMO-LUMO gap, hence

shorter peak absorption wavelength, than in the crystalline state.[77] The change in the peak absorption wavelength shows that the unraveling of the crystalline domain, at least partially, has occurred in the P3DT film stretched to a strain ratio of 2.

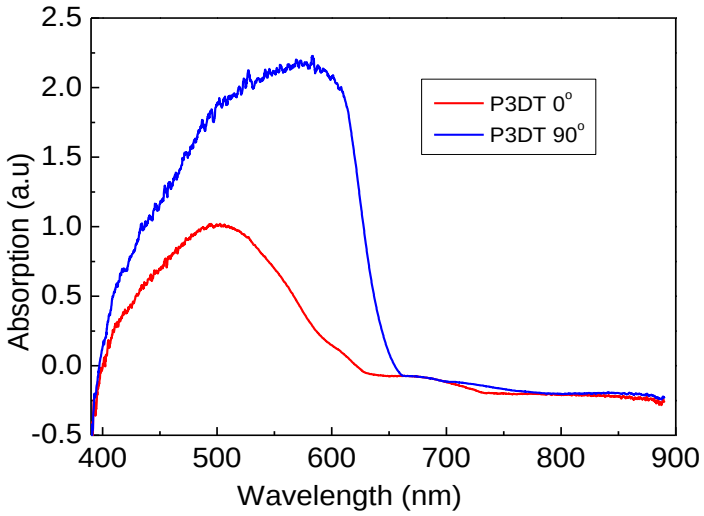

Figure 35. Polarized absorption spectra for the stretched and the original P3DT thin films.

5.3.3 X-ray diffraction spectra of stretched film

The unraveling of the crystalline domain is corroborated by the XRD patterns of the stretched P3DT film (Figure 36). After stretching, the scattering peak shifted from 3.8° for the original P3DT film to 3.6° for the stretched film. Since the 2θ angle is correlated to the spacing (d) between the crystal faces through $2d \sin\theta = n\lambda$, where λ is the wavelength of the X-ray. Smaller θ indicates a larger d for the stretched thin

film, showing that the crystalline domain is expanded by the stretching. The scattering peak still exists in the stretched film, indicating the unraveling of the crystalline domain is only partial.

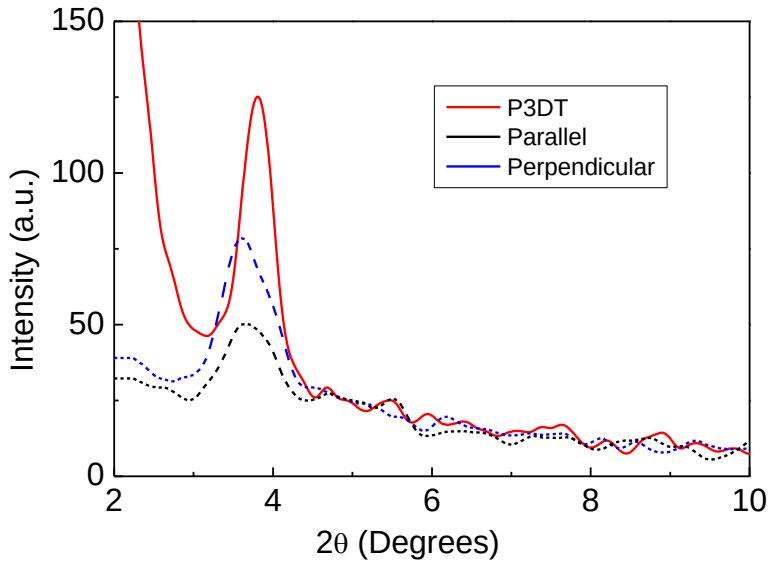

Figure 36. X-ray diffraction of the original and the stretched P3DT films.

5.3.4 OTFTs based on stretched P3DT

The current-voltage characteristics of the fabricated OTFTs with the channel aligned parallel and perpendicular to the stretching direction are shown in Figure 37(a) and (b), respectively. When the channel was parallel to the stretching direction, a much larger current was obtained, as compared to the case where the channel was perpendicular to the stretching direction. Considering all device parameters are the same in the two cases, the larger current can only originate from higher carrier

mobility in the parallel device. The field-effect mobility was determined from the linear region of the I-V curves.[27] The holes moving along the stretching direction has a mobility of $1.69\times10^{-3}cm^2V^{-1}S^{-1}$, which is 20 times higher compared to the results reported for the un-stretched sample (8×10^{-5} cm^2V^{-1} S^{-1}) [3]. For holes traveling in the perpendicular direction, the mobility is 4.1×10^{-4} $cm^2V^{-1}S^{-1}$. The ratio of hole mobility between the parallel and the perpendicular directions is about 4.

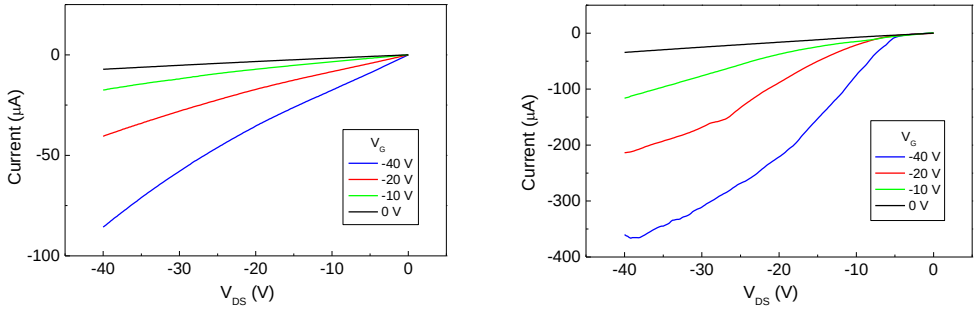

Figure 37. IDS versus VDS characteristics of the OTFTs based on the stretch-oriented P3DT. The longitudinal direction of the channel (from source to drain) is (a) parallel and (b) perpendicular to the stretching direction.

Long chain conjugated polymers have π-bonding that are delocalized along the chain. The bottle neck of carrier transport in conjugated polymers is the slow hopping steps across the disordered amorphous regions. Chain extension and alignment in the amorphous region may lower the disorder, thus the energy barrier for carrier hopping, in the stretched film, leading to an overall carrier mobility increase despite of the

slight damage of the crystalline domain as indicated by the polarized absorption spectra and the XRD pattern of the stretched film. Due to the bulky side groups in the P3DT molecules, in-plane inter-chain π-stacking may be hindered in the direction perpendicular to stretching. Thus a lower hole mobility is observed for holes traveling in the perpendicular direction.

It should be noted that the final chain conformation in the stretched semicrystalline thin film may depend on the strain ratio because the amorphous region is stretched before the crystalline domain. Once the crystalline domain starts to unravel, the benefit of mobility increase brought by the ordering of the amorphous region may be negated by the mobility decrease in the crystalline domain. An optimal drawing ratio exists for achieving the biggest improvement in carrier transport. Further studies are necessary to reveal the correlation between the mobility enhancement and the strain ratio of the drawing. Nonetheless, the observation here indicates stretching is a highly effective method in improving the carrier transport in conjugated polymers.

5.4 Conclusion

In this work, P3DT thin films were stretched by a facile method and their optical, photophysical and electrical properties were investigated. The ordering of the polymer chains imparts strong optical birefringence to the stretched film. The blue shift of the absorption peak and the lowering of the scattering angle in the XRD pattern of the stretched P3DT thin film indicate that the unraveling of the polymer chains in the crystalline domain occurred when the film was drawn to a strain ratio of

2. The field-effect hole mobility increases in the stretched film, which can be attributed to the lowering of the energy barrier height for carrier hoping across the disordered region. Hole mobility anisotropy is also observed in the stretched P3DT film, with a higher carrier mobility along the stretching direction than the perpendicular direction. Being able to be stretched easily with controlled drawing ratio, P3DT can be used as the model system to investigate the conformation variation and its impact on material properties. Such information is useful in determining the most optimal chain conformation to achieve highest performance for polymer electronics.

In this chapter, the mobility of poly (3-decylthiophene) (P3DT) films was enhanced by stretch orientation process. The organic thin film transistor (OTFT) was fabricated by elongating P3DT polymer film to a final length two times to its initial dimension. For this degree of orientation, the intensity ratio between parallel and perpendicular is 2.4. The carrier mobility in thin-film transistors because of the chain alignment have been increased three times by the mechanical stretching process. The mobility in the parallel and perpendicular direction also shows 10 times difference.

CHAPTER VI

TRANSFER A SILICON LAYER ONTO A FLEXIBLE SUBSTRATE

6.1 Introduction

A new layer splitting process – the "Smart-cut" [85] has greatly impact the microelectronic device fabrication, as a mainstream technique to fabricate SOI wafers. That is due to transistors based on SOI wafers are much faster, and the buried insulation layers can also be used to enhance devices stabilities in harsh environments involving particle irradiation or high temperatures.

6.2 Experiment details

The top Si layer was n-type doped (20-50 Ohm·cm) and <100> oriented with a thickness of 320 nm. The buried SiO_2 layer is about 3 micron thick. First, AZ514 photoresist was spin coated on the sample. Then prebaking at 110 ℃ for 1 minute was used to increase the sensitivity of photoresist to UV light. Samples were exposed to UV light by using Karl Suss MA-6 Mask Aligner under a power density of 7.2 mw/cm^2, followed by baking at 120 ℃ for 3 minutes. The exposure to MA6 was repeated under a power of 399 mw, followed by cleaning in acetone for about 20 seconds. Silicon etching was realized by using 20% KOH at 80℃ for about 1.5 minutes, as Figure 38 shown.

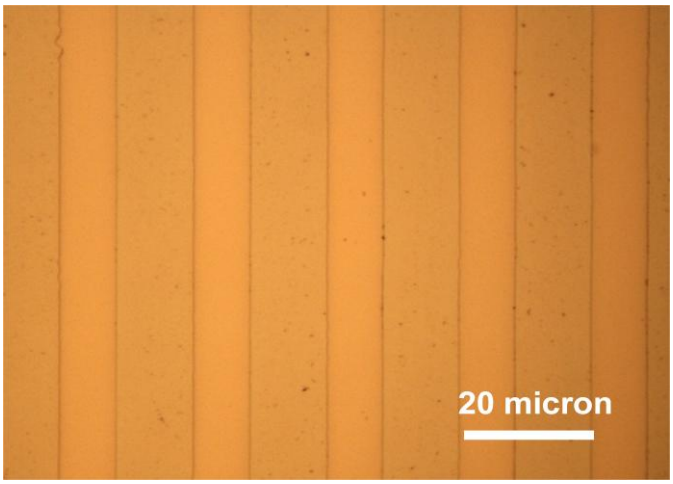

Figure 38. Optical image of a 10 micron patterned SOI.

Then, the buried SiO_2 layer was etched by dipping the wafer into 49% HF. Figure 39 shows the optical image of the structure after etching in HF for about 1 minute. The etching rate is round 1.5 micron per minute. The arrows in Figure 39a and 39b correspond to the region with residual SiO_2 left since etching times were not long enough. Figure 39b shows the optical image of the HF-etched structured for an etching period of 3 minutes. With increasing etching times, the thickness of the residual SiO_2 was reduced down to ~1 micron.

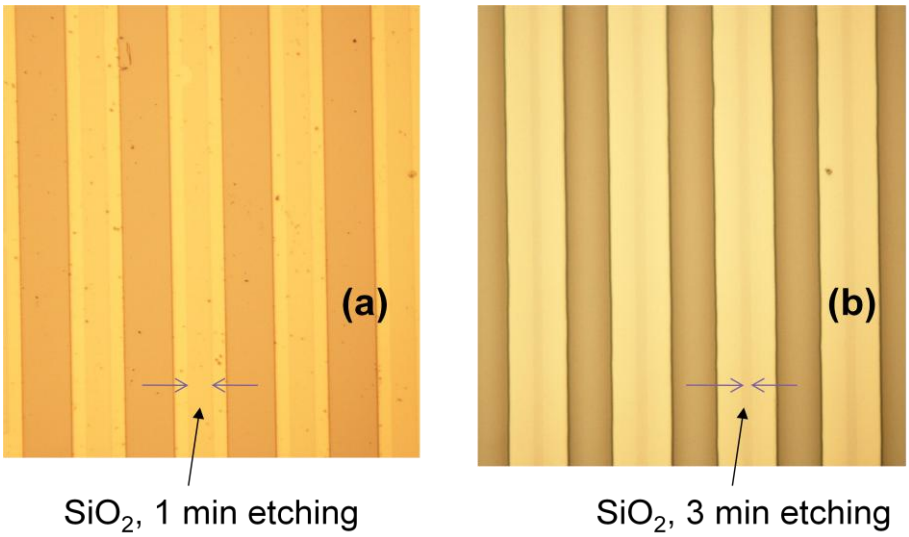

Figure 39. Optical images of etched samples in HF for 1minute and for 3 minutes.

Figure 40 shows the cross sectional view of a cleaved structure obtained by using a scanning electron microscope. In order to make the top Si layer visible, the sample has an incomplete SiO_2 etching, so the residual SiO_2 can support the top Si layer.

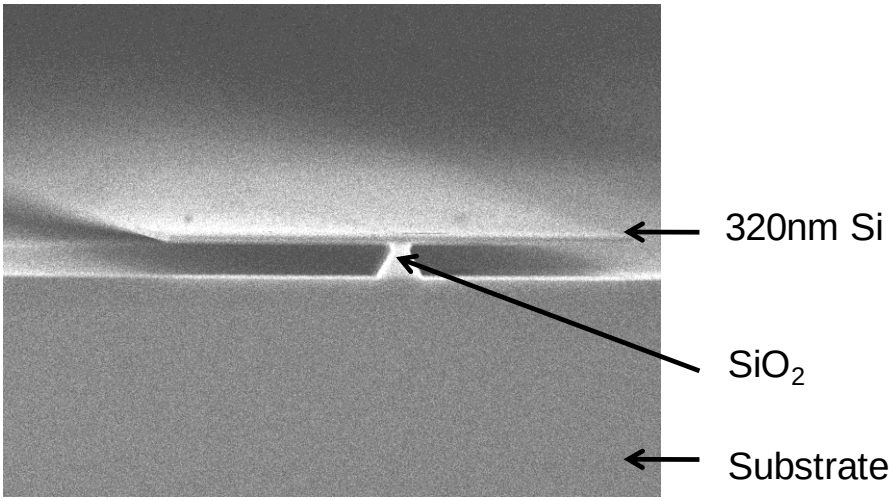

Figure 40. SEM image of the sample after HF etching.

Figure 41 shows the structure transferred onto polydimethylsiloxane (PDMS). PDMS is a silicon-based organic polymer and has very flexible polymer backbones. A thick rubber semi-solid of PDMS can be used as flexible substrate for the proposed device. The dark region in the figure corresponds to the PDMS substrate. The residual SiO_2 is visible as a narrow line, which can be easily removed by HF.

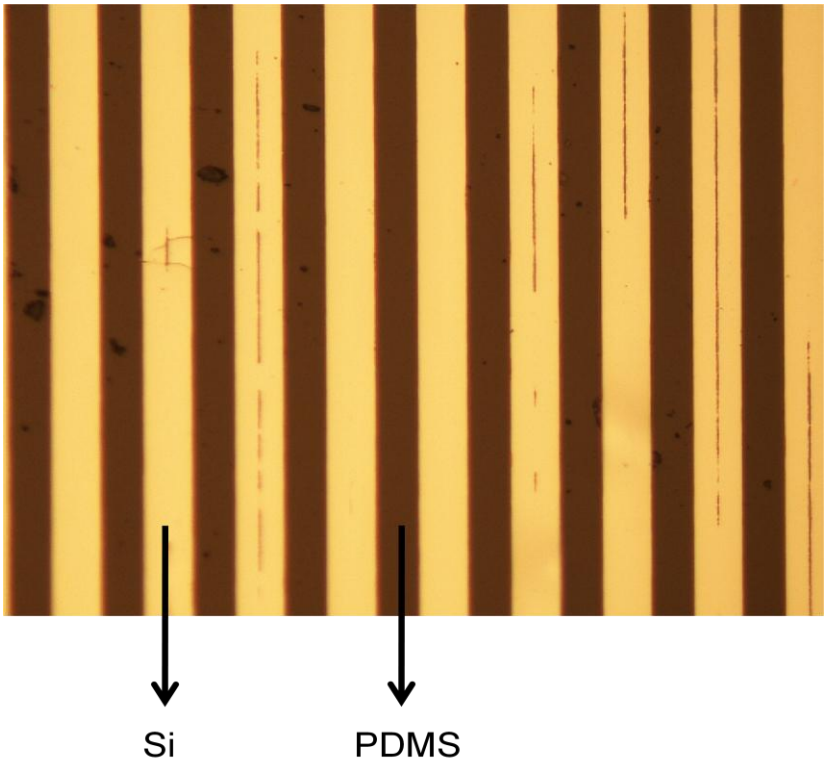

Figure 41. Optical image of the structure with Si stripes bonded with PDMS substrate.

6.3 Conclusion

The study so far has shown the feasibility to transfer a thin Si layer onto a flexible PDMS substrate. With appropriate lithography and Si etching, trenches were

developed and penetrated into the buried SiO_2 layer, thus providing paths for HF solution to etch SiO_2 so that the layer can be lifted off and transferred onto the PDMS substrate.

CHAPTER VII

SUMMARY

The versatility in tuning semiconducting polymer electronic and optical properties by manipulating molecular structure through chemical synthesis has created a huge variety of conjugated polymers. This allows for intelligent material design to achieve best performance for specific applications. Current and future device applications of semiconducting polymers include light-emitting diodes (OLED), thin film transistors (OTFT), photovoltaic cells (OPV), chemical and biological sensors, photodetectors, lasers, and memory devices. The performance of conjugated polymer devices depends on two major factors: the chain conformation in polymer film and the device structure. Highly ordered chain structure usually leads to much improved performance by enhanced interchain interaction to facilitate carrier transport.

The motivation of my work is to address these two major factors in polymer electronics with the nanoimprint lithography. The first work I did is the development of chain ordering functional materials transistor by nanoimprint lithography. I started with highly doped p-type silicon and first deposited 100nm silicon dioxide as the gate dielectric. Then I defined the source and drain region and deposited metal and finished lift-off process. After that, the P3HT was deposited and nanoimprint was applied on P3HT to change the material properties. Finally, I put some Aluminum contact on the highly doped p-type silicon as gate contact.

The chain orientation can be tested by XRD, Polarized microscope and Polarized absorption spectra. I found that there is some polymer chain orientation in the patterned nanostructure, which means the amorphous P3HT can become into crystal P3HT. Finally I made a transistor and measured the mobility of P3HT. In the patterned P3HT area where the chain orientation happens, the mobility increased around 10 times, compared with the un-patterned P3HT which does not have chain orientation.

The second work is based on the discovery in the first work, which is to develop step-and-repeat thermal nanoimprint technique for large-scale. In the patterned functional polymer region, the part of polymer can become into crystal phase from the amorphous phase. The following nanoimprint on other areas will not damage the first nanoimprint pattern. Based on the discovery, we can use a small mold to pattern large area by step and repeat. Another advantage is that the temperature is kept constant. The nanoimprint can be performed again and again without the heating and cooling cycles. That can improve the nanoimprint efficiency.

To fully capitalize on the benefits of nanoscale organic devices such as better performance and higher integration density, it is also indispensable to study the polymer flow distribution in the nanoimprint process, which determines the accuracy of the final geometry and the chain conformation of the imprinted nanostructures. The actual chain orientation of molecular groups in polymer micro- and nanostructures are is complicated, but it this information is crucial for controlling understanding the chemical properties and controlling the physical properties of polymeric materials. To understand how nanoimprint affects polymer chain configuration, Raman spectroscopy is used to

investigate chain conformation change after nanoimprint. The third work is the systematic investigation of polymer chain configuration by Raman spectroscopy to understand how nanoimprint process parameters, such as mold pattern size, temperature, and polymer molecular weight, affects polymer chain configuration. The results indicate that chain orientation in nanoimprinted polymer nanostructures is highly related to the nanoimprint temperature and the dimensions of the mold structures.

In this work, I used PMMA to investigate the polymer chain conformation after nanoimprint. For example, I studied how the nanoimprint processing time affects chain ordering. I compared the Raman of different molecular weight, 15k, 75k PMMA and I found that the higher molecular weight sample shows greater polarization ratio. Third, I compared the different grating dimensions. I also investigated how the residual layer removal step affects the chain orientation in the final polymer structures patterned by nanoimprint.

This research proposes the development of nanoimprint techniques to address three challenging topics: Nanoscale conjugated polymer structures may possess enhanced material performance compared to uniform thin films; the ability to achieve large-area nanoimprint at a low cost level and Raman spectroscopy study to provide information on chain folding and orientation in individual polymer micro- and nanostructures.

REFERENCES

[1] L. R. Bao, X. Cheng, X. D. Huang, L. J. Guo, S. W. Pang, A. F. Yee, J Vac Sci Technol B 2002, 20, 2881.

[2] S. Y. Chou, P. R. Krauss, P. J. Renstrom, Appl Phys Lett 1995, 67, 3114.

[3] X. Cheng, D. W. Li, L. J. Guo, Nanotechnology 2006, 17, 927.

[4] M. Otto, M. Bender, F. Richter, B. Hadam, T. Kliem, R. Jede, B. Spangenberg, H. Kurz, Microelectron Eng 2004, 73-74, 152.

[5] J. Choi, K. Nordquist, A. Cherala, L. Casoose, K. Gehoski, W. J. Dauksher, S. V. Sreenivasan, D. J. Resnick, Microelectron Eng 2005, 78-79, 633.

[6] M. Komori, H. Uchiyama, H. Takebe, T. Kusuura, K. Kobayashi, H. Kuwahara, T. Tsuchiya, J Micromech Microeng 2008, 18.

[7] Y. F. Ding, H. W. Ro, K. J. Alvine, B. C. Okerberg, J. Zhou, J. F. Douglas, A. Karim, C. L. Soles, Adv Funct Mater 2008, 18, 1854.

[8] L. J. Guo, Adv Mater 2007, 19, 495.

[9] J. Taniguchi, Y. Tokano, I. Miyamoto, M. Komuro, H. Hiroshima, Nanotechnology 2002, 13, 592; L. Tao, S. Ramachandran, C. T. Nelson, M. Lin, L. J. Overzet, M. Goeckner, G. Lee, C. G. Willson, W. Wu, W. Hu, Nanotechnology 2008, 19.

[10] S. W. Pang, T. Tamamura, M. Nakao, A. Ozawa, H. Masuda, J Vac Sci Technol B 1998, 16, 1145.

[11] F. Hua, Y. G. Sun, A. Gaur, M. A. Meitl, L. Bilhaut, L. Rotkina, J. F. Wang, P. Geil, M. Shim, J. A. Rogers, A. Shim, Nano Lett 2004, 4, 2467.

[12] M. Beck, M. Graczyk, I. Maximov, E. L. Sarwe, T. G. I. Ling, M. Keil, L. Montelius, Microelectron Eng 2002, 61-2, 441.

[13] L. J. Guo, J Phys D Appl Phys 2004, 37, R123.

[14] P. J. Yoo, S. J. Choi, J. H. Kim, D. Suh, S. J. Baek, T. W. Kim, H. H. Lee, Chem Mater 2004, 16, 5000.

[15] A. S. P. Chang, K. J. Morton, H. Tan, P. E. Murphy, W. Wu, S. Y. Chou, IEEE Photonic Tech L 2007, 19, 1457.

[16] M. Beck, F. Persson, P. Carlberg, M. Graczyk, I. Maximov, T. G. I. Ling, L. Montelius, Microelectron Eng 2004, 73-74, 837; T. Nielsen, D. Nilsson, F. Bundgaard, P. Shi, P. Szabo, O. Geschke, A. Kristensen, J Vac Sci Technol B 2004, 22, 1770.

[17] W. Y. Chen, R. Grover, T. A. Ibrahim, V. Van, W. N. Herman, P. T. Ho, IEEE Photonic Tech L 2004, 16, 470.

[18] D. Pisignano, L. Persano, G. Gigli, P. Visconti, T. Stomeo, M. De Vittorio, G. Barbarella, L. Favaretto, R. Cingolani, Nanotechnology 2004, 15, 766; M. Belotti, M. Galli, D. Bajoni, L. C. Andreani, G. Guizzetti, D. Decanini, Y. Chen, Microelectron Eng 2004, 73-74, 405.

[19] P. Rabiei, W. H. Steier, C. Zhang, L. R. Dalton, J Lightwave Technol 2002, 20, 1968.

[20] L. J. Guo, X. Cheng, C. F. Chou, Nano Lett 2004, 4, 69.

[21] Y. Yi, M. Nakata, A. R. Martin, N. A. Clark, Appl Phys Lett 2007, 90; X. M. Yan, S. Kwon, A. M. Contreras, J. Bokor, G. A. Somorjai, Nano Lett 2005, 5, 745; I.

Gur, N. A. Fromer, C. P. Chen, A. G. Kanaras, A. P. Alivisatos, Nano Lett 2007, 7, 409; L. Zhang, S. Ducharme, J. Li, Appl Phys Lett 2007, 91.

[22] S. Y. Chou, P. R. Krauss, W. Zhang, L. J. Guo, L. Zhuang, J Vac Sci Technol B 1997, 15, 2897.

[23] Z. J. Zheng, K. H. Yim, M. S. M. Saifullah, M. E. Welland, R. H. Friend, J. S. Kim, W. T. S. Huck, Nano Lett 2007, 7, 987.

[24] A. J. Heeger, Angew Chem Int Edit 2001, 40, 2591; A. G. MacDiarmid, Reviews of Modern Physics 2001, 73, 701.

[25] G. Weder, P. Smith, Abstr Pap Am Chem S 2000, 219, U544; M. A. Khan, W. Xu, Khizar-ul-Haq, X. W. Zhang, Y. Bai, X. Y. Jiang, Z. L. Zhang, W. Q. Zhu, J Phys D Appl Phys 2008, 41; Z. Bao, A. J. Lovinger, A. Dodabalapur, Appl Phys Lett 1996, 69, 3066; G. Li, J. Shinar, Appl Phys Lett 2003, 83, 5359.

[26] W. M. Arden, Curr Opin Solid St M 2002, 6, 371.

[27] C. D. Dimitrakopoulos, D. J. Mascaro, Ibm J Res Dev 2001, 45, 11.

[28] B. J. Schwartz, Annu Rev Phys Chem 2003, 54, 141.

[29] T. A. Chen, X. M. Wu, R. D. Rieke, J Am Chem Soc 1995, 117, 233.

[30] I. Mcculloch, M. Heeney, C. Bailey, K. Genevicius, I. Macdonald, M. Shkunov, D. Sparrowe, S. Tierney, R. Wagner, W. M. Zhang, M. L. Chabinyc, R. J. Kline, M. D. Mcgehee, M. F. Toney, Nat Mater 2006, 5, 328.

[31] J. Kim, T. M. Swager, Nature 2001, 411, 1030.

[32] C. Y. Chi, G. Lieser, V. Enkelmann, G. Wegner, Macromol Chem Physic 2005, 206, 1597.

[33] G. L. W. Cross, J Phys D Appl Phys 2006, 39, R363.

[34] G. Kumaraswamy, J Macromol Sci-Pol R 2005, C45, 375.

[35] H. D. Rowland, A. C. Sun, P. R. Schunk, W. P. King, J Micromech Microeng 2005, 15, 2414.

[36] T. Nishino, M. Meguro, K. Nakamae, M. Matsushita, Y. Ueda, Langmuir 1999, 15, 4321.

[37] C. D. Dimitrakopoulos, P. R. L. Malenfant, Adv Mater 2002, 14, 99.

[38] N. C. Greenham, X. G. Peng, A. P. Alivisatos, Phys Rev B 1996, 54, 17628.

[39] P. Dyreklev, G. Gustafsson, O. Inganas, H. Stubb, Solid State Commun 1992, 82, 317.

[40] G. Gustafsson, O. Inganäs, H. Österholm, J. Laakso, Polymer 1991, 32, 1574.

[41] P. Dyreklev, M. Berggren, O. Inganas, M. R. Andersson, O. Wennerstrom, T. Hjertberg, Adv Mater 1995, 7, 43.

[42] H. Park, H. F. Li, X. Cheng, J Vac Sci Technol B 2007, 25, 2325; H. Schift, J Vac Sci Technol B 2008, 26, 458.

[43] E. A. Costner, M. W. Lin, W. L. Jen, C. G. Willson, Annu Rev Mater Res 2009, 39, 155.

[44] S. Y. Chou, P. R. Krauss, P. J. Renstrom, Science 1996, 272, 85.

[45] J. Haisma, M. Verheijen, K. vandenHeuvel, J. vandenBerg, J Vac Sci Technol B 1996, 14, 4124.

[46] S. Johnson, R. Burns, E. K. Kim, G. Schmid, M. Dickey, J. Meiring, S. Burns, N. Stacey, C. G. Willson, D. Convey, Y. Wei, P. Fejes, K. Gehoski, D. Mancini, K. Nordquist, W. J. Dauksher, D. J. Resnick, J Photopolym Sci Tec 2004, 17, 417.

[47] D. Cui, H. Li, H. Park, X. Cheng, J Vac Sci Technol B 2008, 26, 2404.

[48] M. Aryal, K. Trivedi, W. C. Hu, Acs Nano 2009, 3, 3085; Z. J. Hu, G. Baralia, V. Bayot, J. F. Gohy, A. M. Jonas, Nano Lett 2005, 5, 1738; Z. J. Hu, B. Muls, L. Gence, D. A. Serban, J. Hofkens, S. Melinte, B. Nysten, S. Demoustier-Champagne, A. M. Jonas, Nano Lett 2007, 7, 3639.

[49] J. D. Xu, L. Locascio, M. Gaitan, C. S. Lee, Anal Chem 2000, 72, 1930; F. X. Zhang, H. Y. Low, Nanotechnology 2006, 17, 1884.

[50] D. Y. Khang, H. Yoon, H. H. Lee, Adv Mater 2001, 13, 749.

[51] D. Pisignano, L. Persano, P. Visconti, R. Cingolani, G. Gigli, G. Barbarella, L. Favaretto, Appl Phys Lett 2003, 83, 2545.

[52] P. S. Hong, H. H. Lee, Appl Phys Lett 2003, 83, 2441; E. Mele, F. Di Benedetto, L. Persano, R. Cingolani, D. Pisignano, Nano Lett 2005, 5, 1915.

[53] S. Harrer, J. K. W. Yang, G. A. Salvatore, K. K. Berggren, F. Ilievski, C. A. Ross, IEEE T Nanotechnol 2007, 6, 639.

[54] C. Chu, G. N. Parsons, J Vac Sci Technol B 2006, 24, 818.

[55] L. Tan, Y. P. Kong, S. W. Pang, A. F. Yee, J Vac Sci Technol B 2004, 22, 2486.

[56] M. T. Shaw, Annu Rev Mater Sci 1980, 10, 19.

[57] D. G. Yao, P. Nagarajan, Polym Eng Sci 2004, 44, 1998; J. M. Andrews, I. M. Ward, J Mater Sci 1970, 5, 411; P. Nagarajan, D. Yao, J Appl Polym Sci 2005, 96, 764.

[58] C. S. Lee, G. S. Y. Yeh, R. M. Caddell, Mater Sci Eng 1972, 10, 241; M. Nagai, K. Nakamura, H. Uehara, T. Kanamoto, Y. Takahashi, T. Furukawa, J Polym Sci Pol Phys 1999, 37, 2549.

[59] S. Hugger, R. Thomann, T. Heinzel, T. Thurn-Albrecht, Colloid & Polymer Science 2004, 282, 932.

[60] R. L. Jones, T. J. Hu, C. L. Soles, E. K. Lin, R. M. Reano, D. M. Casa, Nano Lett 2006, 6, 1723; Y. F. Ding, H. W. Ro, J. F. Douglas, R. L. Jones, D. R. Hine, A. Karim, C. L. Soles, Adv Mater 2007, 19, 1377; H. J. Patrick, T. A. Germer, Y. F. Ding, H. W. Ro, L. J. Richter, C. L. Soles, Appl Phys Lett 2008, 93.

[61] H. Yoon, H. S. Cho, K. Y. Suh, K. Char, Nanotechnology 2010, 21.

[62] S. H. Ahn, L. J. Guo, Adv Mater 2008, 20, 2044; H. J. Kim, M. Almanza-Workman, B. Garcia, O. Kwon, F. Jeffrey, S. Braymen, J. Hauschildt, K. Junge, D. Larson, D. Stieler, A. Chaiken, B. Cobene, R. Elder, W. Jackson, M. Jam, A. Jeans, H. Luo, P. Mei, C. Perlov, C. Taussig, J Soc Inf Display 2009, 17, 963.

[63] M. T. Li, J. A. Wang, L. Zhuang, S. Y. Chou, Appl Phys Lett 2000, 76, 673.

[64] M. D. Austin, H. X. Ge, W. Wu, M. T. Li, Z. N. Yu, D. Wasserman, S. A. Lyon, S. Y. Chou, Appl Phys Lett 2004, 84, 5299.

[65] D. Cheyns, K. Vasseur, C. Rolin, J. Genoe, J. Poortmans, P. Heremans, Nanotechnology 2008, 19.

[66] M. G. Kang, M. S. Kim, J. S. Kim, L. J. Guo, Adv Mater 2008, 20, 4408.

[67] H. C. Scheer, H. Schulz, Microelectron Eng 2001, 56, 311; J. H. Jeong, Y. S. Choi, Y. J. Shin, J. J. Lee, K. T. Park, E. S. Lee, S. R. Lee, Fiber Polym 2002, 3, 113; L. J. Heyderman, H. Schift, C. David, J. Gobrecht, T. Schweizer, Microelectron Eng 2000, 54, 229; H. C. Scheer, N. Bogdanski, M. Wissen, T. Konishi, Y. Hirai, J Vac Sci Technol B 2005, 23, 2963.

[68] H. D. Rowland, W. P. King, J Micromech Microeng 2004, 14, 1625.

[69] S. Damoun, R. Papin, G. Ripault, M. Rousseau, J. C. Rabadeux, D. Durand, J Raman Spectrosc 1992, 23, 385.

[70] J. H. Nobbs, D. I. Bower, I. M. Ward, Polymer 1976, 17, 25.

[71] N. E. Schlotter, J. F. Rabolt, J Phys Chem-Us 1984, 88, 2062.

[72] J. Purvis, D. I. Bower, Polymer 1974, 15, 645; H. A. Willis, V. J. I. Zichy, P. J. Hendra, Polymer 1969, 10, 737.

[73] M. Suzuki, H. Kato, S. Wakumoto, J Dent Res 1991, 70, 1092.

[74] T. A. Skotheim, J. R. Reynolds, *Conjugated Polymers: Processing and applications*, CRC, Boca Raton, Fla. ; London 2007; Z. Bao, J. J. Locklin, *Organic field-effect transistors*, CRC Press, Boca Raton 2007; E. Reichmanis, H. Katz, C. Kloc, A. Maliakal, Bell Labs Technical Journal 2005, 10, 87; T. B. Singh, N. S. Sariciftci, Annu. Rev. Mater. Res. 2006, 36, 199; H. E. Katz, J. Huang, Annu. Rev. Mater. Res. 2009, 39, 71; H. Sirringhaus, Adv. Mater. 2005, 17, 2411.

[75] B. J. Schwartz, Annual Review of Physical Chemistry 2003, 54, 141.

[76] J. C. Wittmann, P. Smith, Nature 1991, 352, 414.

[77] T.-A. Chen, X. Wu, R. D. Rieke, J. Am. Chem. Soc. 1995, 117, 233.

[78] Z. Zheng, K. H. Yim, M. S. M. Saifullah, M. E. Welland, R. H. Friend, J. S. Kim, W. T. S. Huck, Nano Lett. 2007, 7, 987.

[79] C. Chi, G. Lieser, V. Enkelmann, G. Wegner, Macromolecular Chemistry and Physics 2005, 206, 1597; A. Bolognesi, C. Botta, D. Facchinetti, M. Jandke, K. Kreger, P. Strohriegl, A. Relini, R. Rolandi, S. Blumstengel, Adv. Mater. 2001, 13, 1072; A. Bolognesi, C. Botta, M. Martinelli, W. Porzio, Organic Electronics 2000, 1, 27.

[80] R. Joseph Kline, M. D. McGehee, M. F. Toney, Nat. Mater. 2006, 5, 222.

[81] D. Comoretto, G. Dellepiane, F. Marabelli, J. Cornil, D. A. dos Santos, J. L. Bredas, D. Moses, Phys Rev B 2000, 62, 10173; F. Feller, A. P. Monkman, Physical Review B 2000, 61, 13560.

[82] T. W. Hagler, K. Pakbaz, K. F. Voss, A. J. Heeger, Phys Rev B 1991, 44, 8652.

[83] D. Cui, H. Li, H. Park, X. Cheng, J. Vac. Sci. Technol. B 2008, 26, 2404.

[84] W. D. Nesse, *Introduction to Optical Mineralogy*, Oxford University Press, New York 2004.

[85] M. Bruel, Electron Lett 1995, 31, 1201; M. Bruel, B. Aspar, A. J. AubertonHerve, Jpn J Appl Phys 1 1997, 36, 1636; B. Aspar, E. Jalaguier, A. Mas, C. Locatelli, O. Rayssac, H. Moriceau, S. Pocas, A. M. Papon, J. F. Michaud, M. Bruel, Electron Lett 1999, 35, 1024.

VITA

Dehu Cui completed his B.S. in Southwest Jiaotong University, China, in 1998 and his M.S. degree in engineering science and mechanics at Pennsylvania State University in 2006. He entered the doctoral program in electrical engineering at Texas A&M University in January 2007 and received his Ph.D. in December 2011. He can be reached at: Department of Electrical Engineering, 214 Zachry Engineering Center, TAMU 3128, College Station, TX 77843. His email is cuidehu@gmail.com.